Advanced Drug Delivery Reviews 143 (2019) 206–225

Contents lists available at ScienceDirect

Advanced Drug Delivery Reviews

journal homepage: www.elsevier.com/locate/addr

Towards more accurate bioimaging of drug nanocarriers: turning aggregation-caused quenching into a useful tool

Jianping Qi [a,1], Xiongwei Hu [d,1], Xiaochun Dong [a], Yi Lu [a,c], Huiping Lu [b], Weili Zhao [a,c], Wei Wu [a,b,c,*]

[a] Key Laboratory of Smart Drug Delivery of MOE, School of Pharmacy, Fudan University, Shanghai 201203, China
[b] Center for Medical Research and Innovation, Shanghai Pudong Hospital, Fudan University Pudong Medical Center, Shanghai 201399, China
[c] Department of Pharmacy, Shanghai Dermatology Hospital, Shanghai 200443, China
[d] State Key Laboratory of Natural Medicines, School of Pharmacy, China Pharmaceutical University, Nanjing 210009, China

ARTICLE INFO

Article history:
Received 30 December 2018
Received in revised form 4 May 2019
Accepted 29 May 2019
Available online 31 May 2019

Keywords:
in vivo fate
Nanocarriers
Nanoparticles
Drug delivery
Fluorescence
Bioimaging
Aggregation-caused quenching
Environment-responsive
Bodipy
ACQ

ABSTRACT

One of the current challenges in the monitoring of drug nanocarriers lies in the difficulties in discriminating the carrier-bound signals from the bulk signals of probes. Environment-responsive probes that enable signal switching are making steps towards a solution to this problem. Aggregation-caused quenching (ACQ), a phenomenon generally regarded as unfavorable in bioimaging, has turned out to be a promising characteristic for achieving environment-responsiveness and eliminating free-probe interference. So-called ACQ probes emit fluorescence when dispersed molecularly within the carrier matrix but quench immediately and absolutely once they are released into the ambient aqueous environment upon the degradation of the nanocarriers. Therefore, the fluorescence observed represents integral nanocarriers. Based on this rationale, the *in vivo* fates of various nanocarriers have been explored using live imaging equipment, with very interesting findings revealing the role of the particles. The current applications are however restricted to nanocarriers with highly hydrophobic matrices (lipid or polyester nanoparticles) or with a hydrophobic core-hydrophilic shell structure (micelles). The ACQ-based bioimaging strategy is emerging as a promising tool to achieve more accurate bioimaging of drug nanocarriers. This review article provides an overview of the ACQ phenomenon and the rationale for and examples of applications, as well as the limitations of the ACQ-based strategy, with a focus on improving the accuracy of bioimaging of nanoparticles.

Contents

Abbreviations: ACQ, aggregation-caused quenching; AIE, aggregation-induced emission; API, active pharmaceutical ingredient; ARE, average radiation efficiency; BODIPY, 4,4′-difluoro-4-bora-3a,4a-diaza-*s*-indacene; CLSM, confocal laser scanning microscopy; CMC, critical micelle concentration; CMT, critical micelle temperature; DDS, drug delivery system; EPR, enhanced permeation and retention; FaSSIF, fasted-state simulated small intestinal fluid; FeSSIF, fed-state simulated small intestine fluid; FRET, Förster resonance energy transfer; GIT, gastrointestinal tract; GM, glucan microparticle; LBN, lipid-based nanoparticle; NLC, nanostructured lipid carrier; PCL, polycaprolactone; PLGA, poly(lactic-*co*-glycolic acid); PM, polymeric micelle; PN, polymeric nanoparticle; PTCDI, perylene tetracarboxylic acid diimide; QD, quantum dot; ROI, region of interest; SGF, simulated gastric fluid; SLN, solid lipid nanoparticle; UV, ultraviolet.

* Corresponding author at: Key Laboratory of Smart Drug Delivery of MOE, School of Pharmacy, Fudan University, Shanghai 201203, China.
E-mail address: wuwei@shmu.edu.cn (W. Wu).

[1] These authors contribute equally to this article.

https://doi.org/10.1016/j.addr.2019.05.009
0169-409X/

1. Introduction

For decades, drug delivery systems (DDSs) have played an indispensable role in medical treatment, and that role is expected to keep growing in the near future [1]. From the perspective of pharmacotherapy, the goal of drug delivery should be the precise delivery of active pharmaceutical ingredients (APIs) to the targets of the ailment, thereby enhancing the therapeutic efficacy while reducing systemic exposure. Nanomedicines are newcomers to the DDS family with great promises to complete this mission [2–4]. The propagation of nanomedicines in the literature and media speaks to the obsession not only of the academia and industries but also of the public [5–8]. However, a huge gap that exists between the input and productivity of nanomedicines is cooling down this enthusiasm, as efforts are turning out to be of little success. It is still too early to hail the advent of the nanomedicine era, and many are wondering what the bottleneck to successful translation of nanomedicines is.

Unlike conventional formulations, nanomedicines depend on specific nanocarriers-nanosystems missioned to deliver APIs to targets of action-for their functions. In addition to the difficulties in adapting traditional technologies for the production of nanocarrier-based DDSs, there are more challenges yet to overcome, including but not limited to batch size limitations, batch-to-batch variation, potential nanotoxicity and polymer-derived toxicity, a lack of accurate and sensitive characterization measurements, and a lack of relevancy of *in vitro* models [5,6,9]. Fortunately, appropriate measures have been taken to solve these problems. In company with the developments in nanomanufacturing and physicochemical characterization, such obstacles have been or will be overcome step by step [10–12]. One of the biggest current challenges is nevertheless with the scarce knowledge, if not ignorance, of the *in vivo* behaviors of drug nanocarriers. The human body remains a “grey”, near “black” box, to us in regard to the *in vivo* fate of nanocarriers [13]. Without the full unraveling of *in vivo* behaviors (pharmacokinetics, distribution, degradation, elimination, etc.), as well as bio-carrier interactions, we are unable to find ways for optimization and improvement. Even for those “successful” nanomedicine products such as doxorubicin liposomes (Doxil®), paclitaxel albumin nanoparticles (Abraxane®) and paclitaxel polymeric micelles (Genexol-PM®), we still do not know how they function and what will happen to both the drug and the particles following administration *via* various routes.

Researchers have noticed the importance of unraveling the *in vivo* or biological fate of nanocarriers for a long time [14–16]. Nevertheless, it is very hard to monitor the particles *in vivo*. In the past, there was no choice but monitoring the bulk signals of the payloads such as the encapsulated drugs or probes for nanocarrier drug delivery systems. Owing to the ignorance of the role that the particles play *in vivo*, the research and development of nanomedicines are just hit-or-miss trials. The outcome of any optimization effort should be tested by the *in vivo* pharmacological and toxicological effects. It is time-consuming and low in efficiency, wasting tremendous resources. If the nanocarriers could be monitored accurately, the exact roles that the nanocarriers play, as well as the limits that they can reach, could be weighed in time, and measures could be taken as early as possible during the developing pipeline to save time and resources. In addition, if the particles could be monitored quantitatively, the virtual profiles of *in vivo* drug release can be roughly depicted by direct comparison between the profiles of the encapsulated drugs and the particles.

To fully understand the *in vivo* behaviors of drug nanocarriers, we need to track the vehicles closely using either invasive or non-invasive approaches. The preliminary goals would be to not only “see” the particles at work [17–20] but also unravel structural changes *in vivo* [14–16,21,22]. After browsing the literature, it is quite disappointing to find that we just managed to “see” ambiguous images of particles, let alone that the information obtained sometimes is contradictory due to a lack of reliable tools to monitor the particles.

Different from molecular imaging in diagnosis, which is based on the recognition of the bulk signals of probes, bioimaging of nanoparticles detects “particles” whose fundamental properties evolve in the body with time [19,23,24]. Due to the extraordinarily small size, the direct observation of drug nanocarriers in the body is impractical even with the help of microendoscopic tools. The widely used strategy is to collect and analyze certain physical signals from particles or particle compositions or to use some kind of probe embedded within. If the particles or compositions give usable signals, the particles are able to be imaged and analyzed; if not, probes such as isotopes or fluorophores should be used to make the particles detectable [25–27]. It should be marked that the probe signals are mixed signals of both the encapsulated and

released probes, and do not represent exactly the nanocarriers. Only if the probes do not release at all, can the probe signals be used to represent the nanocarriers accurately.

For decades, the application of fluorescent bioimaging in drug delivery has steadily increased [28–32]. Tracking the transport of nanocarriers, especially using fluorescence bioimaging, in both body and cell models has emerged as a trend in recent years. For instance, the demonstration of tumor targeting by ligand-decorated nanocarriers using various bioimaging probes has become a routine [33–35]. Conventional probes for molecular bioimaging are commonly designed to give steadfast and strong signals [36–39]; however, they are not applicable to bioimaging of nanoparticles. The conventional labeling strategies are generally confronted with one big problem-the difficulties in distinguishing the nanocarrier-associated signals from the bulk signals of probes [19]. Steadfast probes give signals no matter whether they are in or out of the nanocarrier matrix. Therefore, the particle-associated signals can hardly be discriminated from the non-associated signals of free or released probes. The fraction of non-associated signals generates interference in the bioimaging of nanoparticles.

Drug nanocarriers are generally labeled through physical embedment or chemical conjugation of the probes with either the carrier materials or the drugs. If the nanocarriers are non-biodegradable (e.g., polystyrene nanoparticles [40,41]), and the labeling is firm enough, the probe signals represent the nanocarriers accurately; however, this is not always the case because drug nanocarriers are usually made to be biodegradable due to safety considerations. Following the degradation of the nanocarrier matrix, the labeling probes should be dissociated from the matrix and released into the ambient environment (Fig. 1). The problem is that free or released probes still give signals (Fig. 1A). What we observe is actually a mix of signals from both nanocarriers and free probes. In Hollins et al.'s study [42], paclitaxel nanocrystals were first labeled by a near-infrared dye, FPI-749 (λ_{ex}/λ_{em} = 750 nm/782 nm), using a platform technology of crystal hybridization developed by the same group, and live imaging revealed the time course of the biodistribution of the nanocrystals following intravenous administration. It was puzzling that the fluorescence could be found in tumors and various tissues for an extended time up to 7 d (Fig. 2), contradicting the common belief that nanocrystals did not last for so long [43,44]. Therefore, the authors gave an explanation that the signals in later stages might be attributed to the released probes rather than the nanocrystals themselves. The signals from free probes make up a majority of the interference and should not be misread as the nanoparticles. The inaccuracy thus heralds the application of new types of environment-responsive probes.

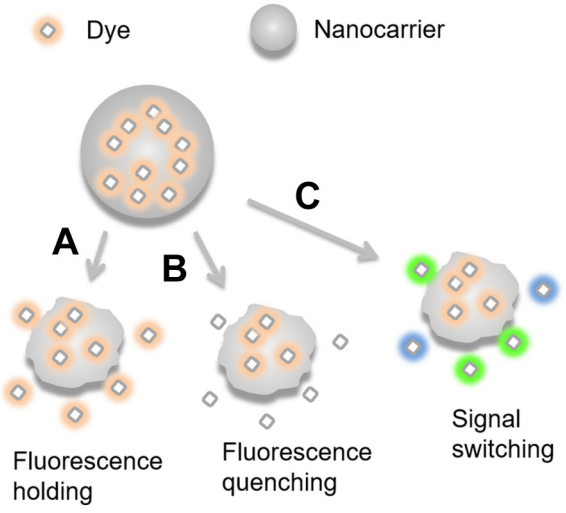

Fig. 1. Schematic presentation of the virtual changes that may happen to the signals of free or released fluorescence probes upon degradation of the nanocarrier matrix. The fluorescence of conventional probes remains unchanged (A), whereas the signals of environment-responsive probes undergo significant changes in response to environmental factors, for example, fluorescence quenching (B) and signal switching (C).

Environment-responsive fluorescent probes are a series of fluorophores whose emission is sensitive to environmental triggers such as pH, solvents, viscosity, enzymes, certain molecules and spatial distance [45–47]. In recent years, there has been a growing number of reports on applications for this kind of new intelligent probes in molecular bioimaging, for instance, in detection of the pathological conditions in tumor tissues [48,49]. The same rationale has been employed to visualize the on-demand release of drugs at target sites in response to triggers in the tumor microenvironment [50–53]. Some types of newly established environment-responsive fluorophores have been reported to show potential in the discrimination of signals from different sources. By using environment-responsive fluorophores to label nanocarriers, the chances of successfully discriminating nanocarrier-associated signals from free-probe signals grow, as well. As illustrated schematically in Fig. 1B & C, upon the degradation of the nanocarrier matrix, the signals of released or free probes change considerably in response to environmental factors. Fluorescence quenching (Fig. 1B) and signal switching (Fig. 1C) are two kinds of changes whose rationales have been successfully employed for the bioimaging of nanoparticles. In this issue, two categories of environment-responsive probes, based on Förster resonance energy transfer (FRET) and aggregation-induced emission (AIE) [54], are reviewed with regard to monitoring the *in vivo* fate or cellular pharmacokinetics of drug nanocarriers. In this article, we present an overview of the advances in another novel kind of environment-responsive fluorescent probe based on the rationale of aggregation-caused quenching (ACQ).

2. Aggregation-caused quenching

2.1. The ACQ phenomenon

Aggregation is a common phenomenon that refers to the formation of clusters of monomers at relatively high concentrations. Driven by intermolecular hydrophobic forces, hydrophobic molecules are prone to form aggregates when being dispersed from a favorable into an unfavorable solvent, such as aqueous solutions [55]. Aggregate systems may appear as homogenous solutions, but the aggregates are actually dispersed, rather than dissolved, in the solvent [56]. Moreover, formed aggregates are very small, enough to maintain thermodynamic and kinetic stability without precipitation [55]. In general, aggregation is an irreversible process, and aggregates will not easily disaggregate once formed except when the environment becomes favorable enough to disrupt the aggregates into monomers again, for instance, when the content of an favorable organic solvent increases to a threshold or when structures with hydrophobic domains (e.g., micelles, proteins, etc.) are introduced into the environment [56].

Fluorophores are generally composed of planar and polycyclic π-conjugated frameworks that establish the basis for high-efficiency luminescence [57,58]. Most fluorophores are hydrophobic because of their aromatic nature, whereas the working environment is generally aqueous. Dispersing fluorophores into aqueous media leads to aggregation due to intermolecular interactions, such as π-π stacking, if the molecules are unable to be dispersed in time [59]. Aggregation commonly results in reduced or quenched fluorescence [59,60]. This phenomenon was discovered by Förster and Kasper approximately half a century ago when they first found the fluorescence of pyrene weakened along with an increase in concentration [61]. Gradually, this behavior proved to be common in most aromatic hydrocarbons and derivatives and was defined by Birk as ACQ in 1970 [55]. By definition, ACQ refers to the phenomenon in which fluorophores that are highly emissive in a dilute solution state become weakly emissive or even non-emissive in an aggregated state [55,59,62,63]. ACQ is generally regarded as unfavorable and remains a hurdle to the application of conventional fluorophores in

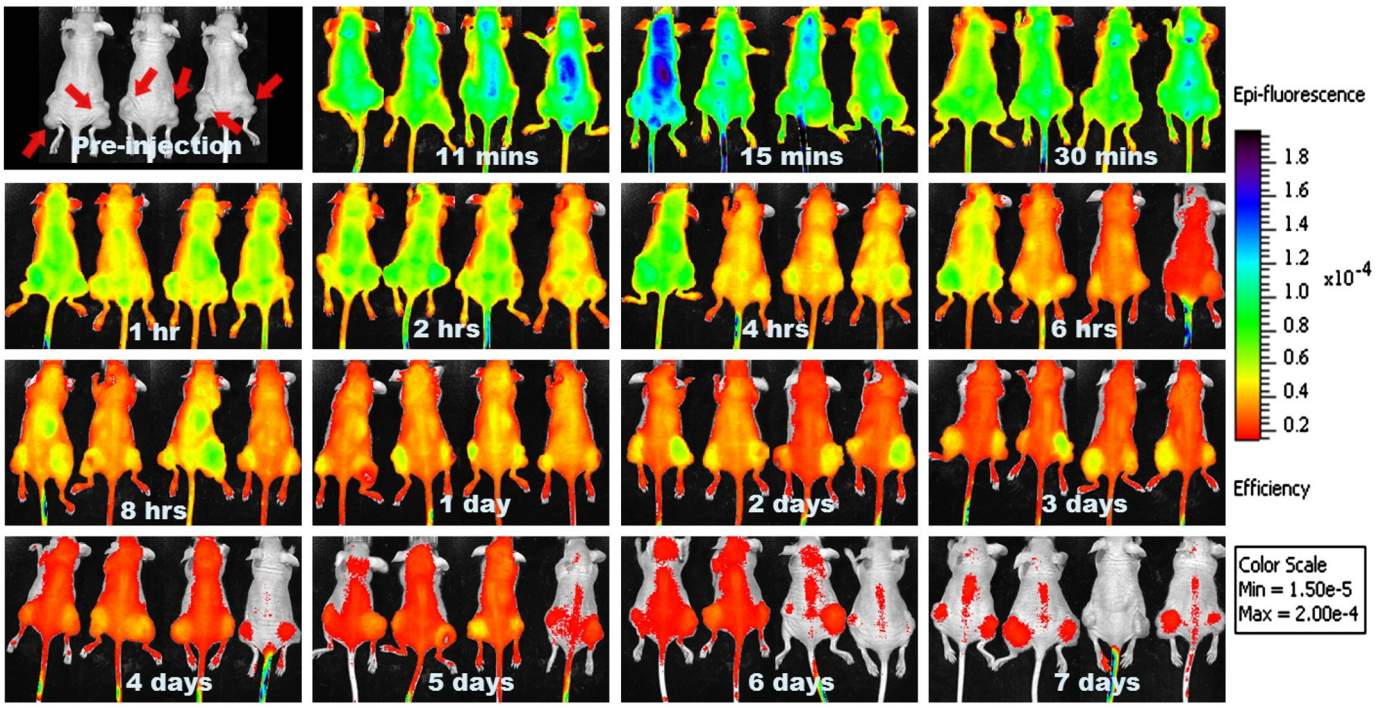

Fig. 2. IVIS live images indicate the biodistribution patterns of paclitaxel nanocrystals, fluorescently hybridized with a near-infrared dye FPI-749, in tumors (hind leg; both sides) and the whole body. Signals are observed for as long as 7 d, apparently contradicting the common belief that nanocrystals dissolve very quickly. The later-stage fluorescence is attributed to free or released probes, rather than the nanocrystals. Reprinted from reference [42] with permission. Copyright 2013 Elsevier.

bioimaging [59,60,63,64]. Any effort to mitigate ACQ has turn out to be of little success because aggregation is a spontaneous and natural process [65–67]. The most prominent adverse impact of ACQ is the fluorescence attenuation that often results in inadequate fluorescence for bioimaging [68]. Moreover, the range of fluorescence linearity is generally very narrow due to ACQ, raising concerns of inaccuracy in molecular bioimaging [69].

As ACQ commonly takes place in aqueous media with hydrophobic fluorophores [70], the correlation between fluorescence intensity and the water content in a system displays the ACQ phenomenon very well (Fig. 3) [71]. When the water content in a binary system increases to a certain threshold (approximately 70% as shown in the upper panel of Fig. 3), the solvating ability of the mixture solvent becomes so poor that most of the dye molecules phase out and become aggregated

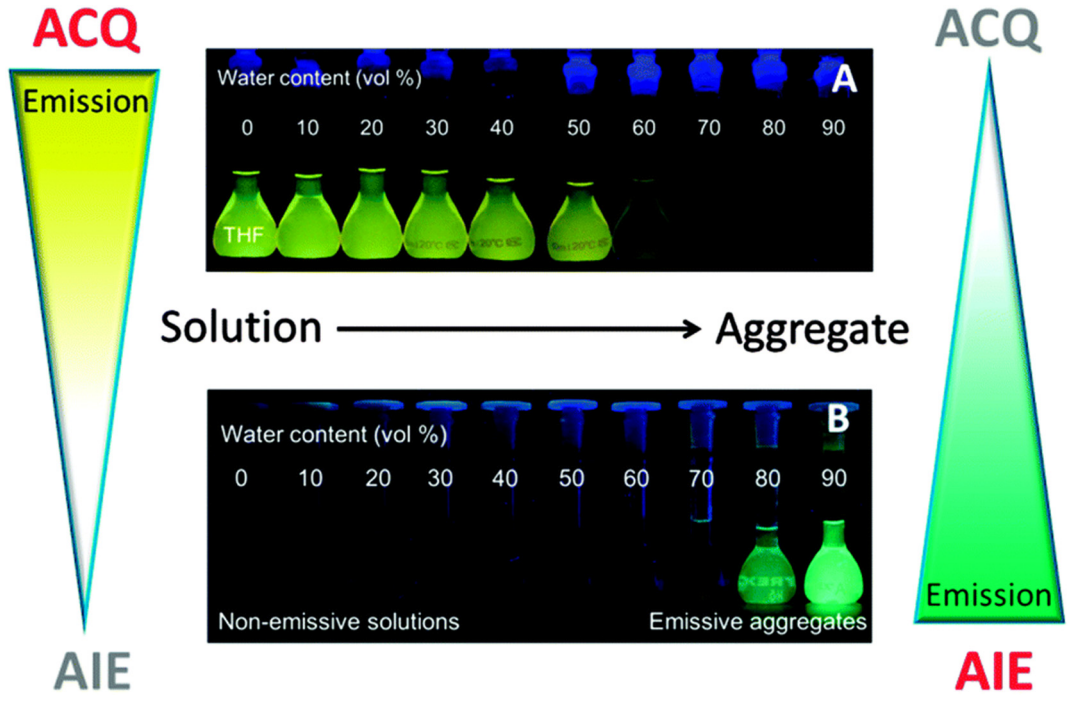

Fig. 3. Visual demonstration of two opposite outcomes in the aggregation of fluorophores when the water content in a binary solvent system (tetrahydrofuran/water) increases to a threshold: ACQ (upper panel) and AIE (lower panel). Reprinted from reference [62] with permission. Copyright 2011 Royal Society of Chemistry.

[72]. As a result, the fluorescence quenches spontaneously. The same is sure to happen when dispersing the fluorophore solution into near-100% aqueous media, such as in a real working environment. Some fluorophores with large planar structures are able to achieve absolute quenching, with fluorescence down to zero, in aqueous environments [19,72]. ACQ may happen through various mechanisms other than desolvating-induced aggregation, such as supramolecular self-organization [73,74], which nevertheless is beyond the discussion of this article. To counter the ACQ effect, as is always done in bioimaging, increasing the dispersity or avoiding the aggregation of fluorophores is workable by certain approaches, such as micellization using surfactants [75].

Although all aromatic fluorophores exhibit ACQ effect, as reported by Birks [55], the quenching efficiency varies according to the molecular structure. The ACQ effect would not be notable if the aromatic rings were non-planar and able to rotate freely. It is very interesting that aggregation sometimes leads to the contrary phenomenon of enhanced luminescence in concentrated solutions or in a solid state. This phenomenon was first discovered by Tang and colleagues and named as AIE [64,71]. AIE dyes are non-emissive or weakly emissive in a dilute solution state but are emissive in an aggregated state or when the rotation of the molecular structure is restrained. AIE fluorophores have been gaining recognition in versatile fields of chemistry and bioimaging in recent years [39,62,71,76–78]. In this issue, Wang et al. provide an overview of the rationale and applications of AIE in the exploration of the biological fate of nanoparticles [54]. Although ACQ and AIE seem merely to have opposite modes of emission (Fig. 3), ACQ is more common than AIE.

2.2. Mechanisms of ACQ

Whereas the apparent mechanism of ACQ is aggregation, the actual mechanism behind is the formation of sandwich-shaped excimers and exciplexes aided by the collisional interaction between aromatic molecules in both excited and ground states [55]. Aggregates with either random or ordered structures are formed through π-π stacking of the planar rings of adjacent fluorophores [79]. The excited states of aggregates often decay *via* non-radiative pathways, immediately causing fluorescence quenching. In addition, some dyes, such as cyanines, undergo self-association at the solid-liquid interface or in solution under the strong drive of intermolecular attractive forces, leading to aggregation in solution and fluorescence quenching [70,80].

The self-association patterns of dyes are affected by media. According to the molecular exciton coupling theory, the hypsochromically shifted H-aggregate (H for hypsochromic) and the bathrochromically shifted J-aggregate (J for Jelly) exhibit distinguished absorption band changes in comparison with that of the monomers (Fig. 4) [81]. Generally, dye molecules stack in parallel by taking end-to-end and plane-to-plane orientations to form two-dimensional J- and H- aggregates, respectively. The dye molecules can be regarded as point dipoles and the excitonic state of the aggregate splits into two levels through the interaction of transition dipoles, according to the exciton theory. Because any two dipoles in an H-aggregate are parallel and the repelling force between them cause a higher energy state (S2 in H-aggregates), the absorption spectrum of the H-aggregate shifts towards the blue [82]. However, for J-aggregates, the syntropic dipoles achieve a lower energy state (S1 in J-aggregates) and result in redshift of the absorption. Although the anti-parallel alignment in H-aggregates may produce a lower energy state (S1 in H-aggregates) and reversed dipoles in J-aggregates may increase the energy of a state (S2 in J-aggregates), they do not have any influence on the shift of the absorption spectrum, as the transition is only allowed for transition dipole moments larger than zero [83]. Practically, the aggregates we get are not absolutely an H- or J-aggregate. The formation of an H-aggregate is frequently driven by the interaction of π-π stacking. Thus, the molecules bearing large conjugated co-planar structures tend to aggregate in this way; otherwise, a J-aggregate co-exists. Normally, the fluorescence of H-aggregate dyes quenches due to the increased demand for excitation energy, which is the main mechanism of ACQ. The H- and J-aggregates exist as a one-dimensional assembly that can be in a brickwork-, ladder- or staircase-type of arrangement [84].

The tendency of aggregation depends on the dye structure, as well as environmental factors, such as the formation of micelles and microemulsions, pH, ionic strength, concentration, solvent polarity, electrolytes and the medium temperature. For a given dye molecular structure, a stacked arrangement is proposed for higher aggregates when the long molecular axis of each molecule is perpendicular to the dye molecules and the aggregate axis within a distance of

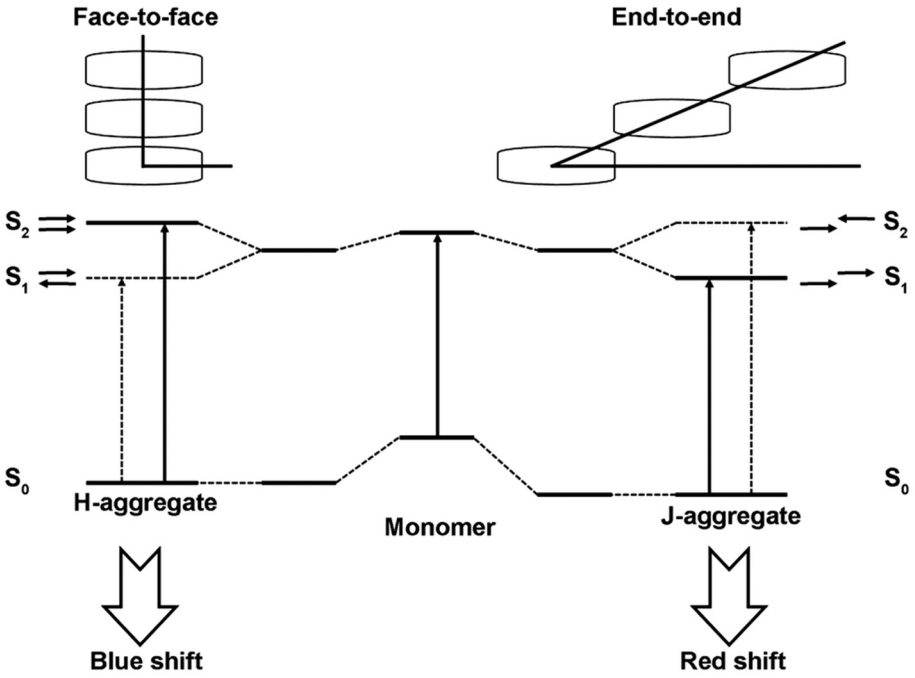

Fig. 4. Schematic presentation of the mechanisms of ACQ. Adapted from reference [81] with permission. Copyright 2014 Royal Society of Chemistry.

approximately 3.3 Å [85]. The formation of J-aggregates is dependent on the compact molecular architecture and high water solubility. The presence of a quencher at very low concentrations quenches J-aggregates [86]. Per the influence of the environment, the medium sometimes can serve as a "glue" for the adhesion of two dispersed molecules because the medium-probe interaction is always stronger than probe-probe interaction [87]. Similarly, this kind of aggregation weakens or quenches the fluorescence.

2.3. Categories of ACQ fluorophores

Most categories of fluorophores exhibit the ACQ effect, but not a single one is designed for that purpose because ACQ is generally not welcome. In Table 1, only a limited number of fluorophores whose applications are closely related to ACQ are listed. The organic molecules that generally possess conjugated planar structure and strong hydrophobicity are the main sources of ACQ fluorophores. Owing to the rigid planar structure formed by four conjugated benzene rings and an ultra-low solubility in water [88], pyrene tends to form excimers/aggregates when the dissolving environment is polarized. On the other hand, it is preferentially solubilized by hydrophobic constructs formed by other molecules as well and has been employed to explore the formation of both vesicular and micellar systems [89,90]. However, the short emission wavelengths of pyrene limit its use in bioimaging. Fluoresceins are a large category of dyes that have been widely used in labeling and tracking. Some of them also present significant ACQ effects and have been utilized to monitor the volume or structural integrity variations by observing the dequenching of fluorescence [91,92]. Cyanines have the distinctive ability to form several types of aggregates, such as H- and J-aggregates, on solid supporting surfaces and in solutions accompanied with a dramatic shift in absorbance and fluorescence quenching [86,93,94]. Perylene tetracarboxylic acid diimide (PTCDI) derivatives are structurally conjugated with five benzene rings and two aza-rings to form a plane and possess an unusual propensity to form self-assembled linear chain structures and aggregates. H-aggregates are formed by the face-to-face arrangement of PTCDI monomers upon dispersal in water and cause fluorescence quenching due to strong intermolecular hydrophobic forces and hydrogen bonding interactions [74]. BODIPYs (4,4′-difluoro-4-bora-3a,4a-diaza-*s*-indacene) are a class of fluorescent dyes with high quantum yields and a photophysical stability that are more superior than those of fluoresceins in complicated biological environments. A series of aza-BODIPY dyes with large conjugated planar structure and near-infrared emission were recently discovered to have an absolute ACQ effect and have been used to explore the *in vivo* fate of various nanocarriers [72,95–97].

Quantum dots (QDs) are inorganic fluorescence substances whose photoluminescence is greatly dependent upon the particle size and surface environment [98,99]. It is very interesting that the aggregation of QDs in aqueous media can cause fluorescence quenching, as well, due to electronic coupling and exciton energy transfer, according to some reports [100–102]. This phenomenon of QDs can also be ascribed to the ACQ effect and might be of potential use.

3. Rationale of ACQ-based bioimaging of nanocarriers

3.1. General rationale

The accurate bioimaging of drug nanocarriers calls for the discrimination of carrier signals from probe signals [19]. Fig. 1B & C schematically demonstrates two workable strategies to address this problem by using environment-responsive probes whose signals attenuate or switch upon the degradation of nanocarriers and the simultaneous probe release [103–105]. By observing the variations in signals (intensity and wavelength), the virtual status of nanocarriers can be inferred. In total, there are three categories of environment-responsive fluorophores (FRET, AIE and ACQ) discussed in this theme issue. Unlike the "on→on" (FRET) and "off→on" (AIE) modes of signal switching, the ACQ strategy takes on an "on→off" mode that proves to be more suitable for the bioimaging of nanocarriers.

Fig. 5A is a schematic demonstration of the rationale for ACQ-based bioimaging with solid lipid nanoparticles (SLNs) as exemplary nanocarriers [72]. The fluorophores for this purpose have a BODIPY or an aza-BODIPY parent structure and emit strong fluorescence in a molecularly dispersed state such as in solution or a nanocarrier matrix. When fluorophores are embedded uniformly within drug nanocarriers, the physical barriers of the nanocarrier matrix prevent the aggregation and subsequent quenching of the fluorophores, thus illuminating the nanocarriers. Owing to their high hydrophobicity, ACQ fluorophores can only be embedded into nanocarriers with a hydrophobic matrix or core. Following the degradation or disintegration of the nanocarriers, the probes are released into the surrounding aqueous environment and immediately form aggregates under the driving force of hydrophobicity [106], causing absolute and instant fluorescence quenching. Therefore, the observed fluorescence signals represent integral nanocarriers, with artifacts due to emission of free probes being substantially reduced. Based on this rationale, the *in vivo* fate of nanocarriers can be explored using live imaging equipment. However, it is worth noting that the above rationale is based on several prerequisites, which will be elaborated below.

A comparison between the ACQ fluorophores and a conventional fluorophore DiR, gives totally different results, highlighting the superiority of ACQ fluorophores (Fig. 5B). The live images obtained by ACQ fluorophores indicate the quick and significant degradation of SLNs in the gastrointestinal tract (GIT), but the fluorescence of the conventional probe group holds for significantly longer periods of time [72]. The mechanism of the fast lipolysis of lipid-based nanocarriers apparently supports the ACQ-based rather than DiR-based live imaging results [107,108].

3.2. General requirements for ACQ fluorophores

Currently, fluorescent bioimaging is developing towards higher accuracies, high sensitivity, speediness, high spatiotemporal resolution and stability [109]. As labeling reagents, ACQ fluorophores should meet some basic requirements besides the ACQ properties, that is, high brightness, high photostability and emission at suitable wavelengths [110]. As the tissue-penetration depth of fluorescence is positively correlated to the wavelength [111], near-infrared fluorescence dyes are preferred. In addition, some commercial instruments have specifications for detection wavelengths; for example, the general wavelength of detection for a confocal laser scanning microscope (CLSM) is less than 650 nm, whereas that for *in vivo* live imaging is generally above 700 nm to reduce the interference of self-luminescence from animal tissues [112]. A high quantum yield is another requirement because ACQ probes should be embedded in trace amounts to avoid concentration quenching. A lack of photostability is a common drawback of conventional fluorophores, which makes the obtained results inaccurate and unreliable [113]. ACQ probes should have a high photostability under any circumstance to meet the requirement for bioimaging.

3.3. Prerequisites for ACQ-based bioimaging

3.3.1. Water sensitivity

The usefulness of ACQ probes in the real-time monitoring of nanocarriers depends primarily on the water sensitivity, i.e., the responsiveness of the probes to water. As fluorescence quenching takes place instantly upon aggregation, the formation of aggregates would be the step that determines water sensitivity [114]. Among multiple factors, chemical structure and hydrophobicity seem to be the predominant factors affecting aggregation [75,88]. Large conjugated coplanar structures favor π-π stacking and thereby aggregation and fluorescence

Table 1
Categories of ACQ fluorophores and fundamental properties.

Name	Chemical structure	$\lambda_{ex}/\lambda_{em}$ (nm/nm)	Properties	Applications	Ref.
Pyrene	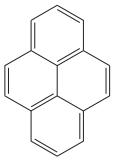	345/378	Solubility in water: 2-3 μM; long life time; efficient formation of excimers in water	Determination of critical micelle concentration	[89,90]
Calcein	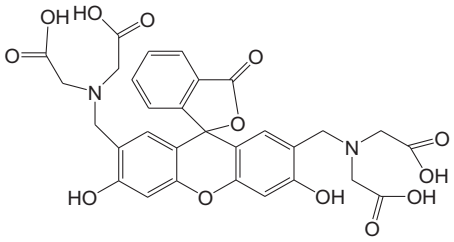	494/517	Hydrophilic; concentration quenching	Measurement of cell volume changes	[92]
5(6)-carboxyfluorescein	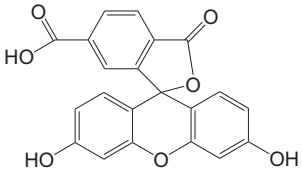	492/517	Hydrophobic; concentration quenching	Liposome-cell interaction monitoring	[91]
Cyanine (F-SLOH)	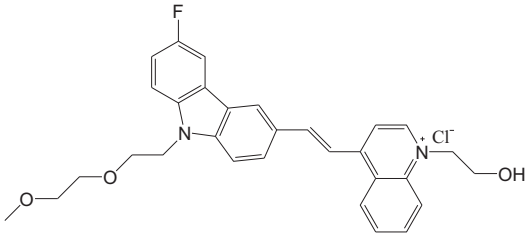	620/636	Hydrophilic; Aβ oligomer selectivity	Early diagnosis and intervention of Alzheimer's disease	[94]
PTCDI	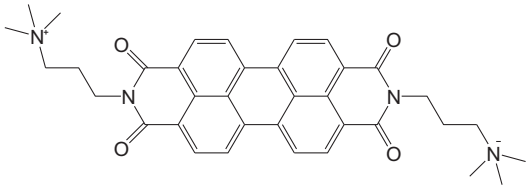	498/550	Hydrophilic; pH-sensitive aggregation quenching	Detection of allosteric control of the DNA I-motif	[74]
Aza-BODIPYs	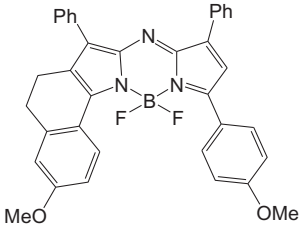	708/732	High quantum yields; good photophysical stability; hydrophobic; absolute ACQ in water	Visualize the in vivo fate of lipid-based nanocarriers	[72]
Graphene QDs		230/420	Fluorescence quenches at pH 1 and restores at pH13	Potential applications in turn-on/off sensors	[100]
CdSe QDs	Mercaptoacetic acid capped	365/590	Fluorescence quenched upon electrolyte induced aggregation	Potential applications in molecular sensing and imaging	[102]
CdTe QDs	Cysteamine capped	461/594	ACQ at high pHs; fluorescence recovery in the presence of F^- ion; high signal-to-background ratios.	Fluoride detection	[101]

QDs: Quantum dots

quenching, while strong hydrophobicity not only accelerates the formation of aggregates but also enhances the coherent force of the aggregates formed [115].

The water sensitivity of ACQ probes is commonly displayed by the responsiveness of the fluorescence to the water content in an organic solvent/water binary system. As demonstrated in Hu et al.'s study, the fluorescence emission spectra of ACQ probes demonstrate decremental fluorescence as a function of water content, which diminishes slowly at early stages but drops abruptly at a threshold (50%-70%), in an acetonitrile/water binary system (Fig. 6A) [72]. A responsive threshold of lower

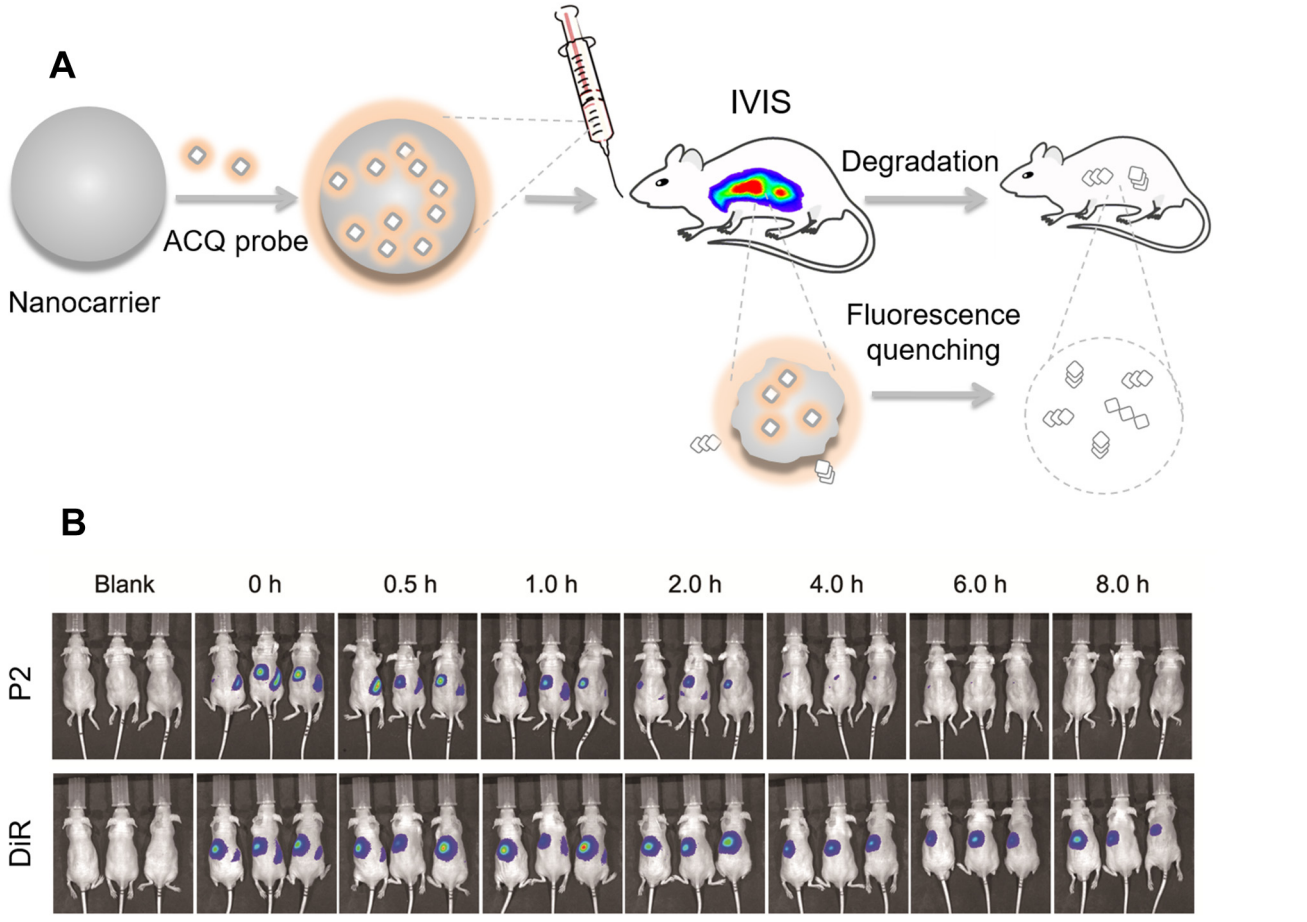

Fig. 5. Schematic demonstration of the general rationale for ACQ-based bioimaging of nanocarriers (A) and a comparison between the ACQ probe P2 and a conventional probe DiR for the capability of monitoring of SLNs more accurately *in vivo* (B). Adapted from reference [72] [97] with permission. Copyright 2015 Elsevier and 2017 American Chemical Society.

water content indicates a higher water sensitivity. An ACQ probe encoded P2 has a responsive threshold at approximately 60%, indicating a high water sensitivity (Fig. 6B) [72].

3.3.2. Fast quenching

The responsive threshold is merely an indicator of the water sensitivity but has little significance in practice because the *in vivo* environment is generally near-100% aqueous, but not absolutely (100%) aqueous due to the presence of endogenous lipids, proteins and so on. When dispersing an organic solution of ACQ probes into an aqueous environment above the water-sensitivity threshold, abrupt fluorescence quenching is sure to happen, as demonstrated in Hu et al.'s study (Fig. 6C & D). Nevertheless, the responding time, or fluorescence quenching speed, matters because any delay in response would require a postponement in the detection and possibly increase the chance of misreading the results. As demonstrated in Fig. 7A, the ACQ-based bioimaging strategy requires the fast quenching of probes once released into an aqueous medium, which means that quenching must occur before the first as-soon-as-possible measurement time point (T_1). In delayed quenching, the fluorescence is unable to drop to its lowest level in time. To adapt to real-time bioimaging, the responsiveness should be as fast as possible; otherwise, delayed quenching would bring about interference, compromising the accuracy of the bioimaging. If there is unavoidable delay in the responsiveness, it should not be later than the first predetermined time point for analysis.

3.3.3. Absolute quenching

To eliminate artifacts, the signals of free probes should be erased upon release from the nanocarriers. Since it is impossible to remove the free probes from the system, the fluorescence quenching should be absolute, with fluorescence down to zero. Fig. 7B demonstrates a comparison between absolute and non-absolute quenching. If quenching is non-absolute, the residual fluorescence presents a source of interference that compromises the accuracy of bioimaging.

However, the ACQ effect is generally not at all absolute. For example, the fluorescence intensity and emission wavelengths of pyrene change but do not disappear when it is dispersed into an aqueous medium [116]. The residual fluorescence results in interference and the misreading of signals, compromising the accuracy of the bioimaging. The absolute-quenching properties of some categories of ACQ probes enable a more accurate monitoring of nanocarriers *in vivo* due to the absolute elimination of free probe-derived interference [117].

3.3.4. Synchronous quenching

The most prominent advantage of ACQ-based bioimaging is the ability to discriminate drug nanocarriers and establish a proportionate correlation between the fluorescence and the amount of integral nanocarriers. Nevertheless, there are some circumstances when fluorescence quenching does not exactly reflect the degradation of the particles. As illustrated in Fig. 7C, synchronous quenching means the fluorescence attenuation keeps a nearly identical pace with the degradation of the nanocarrier matrices, whereas in nonsynchronous quenching, the fluorescence attenuation either outruns or lags behind the degradation of the nanocarriers.

Due to their ultrafine size, it is impossible to recover nanocarriers from biological milieu to measure the *in vivo* degradation kinetics [118]. For this reason, *in vitro* studies in a simulated biological medium

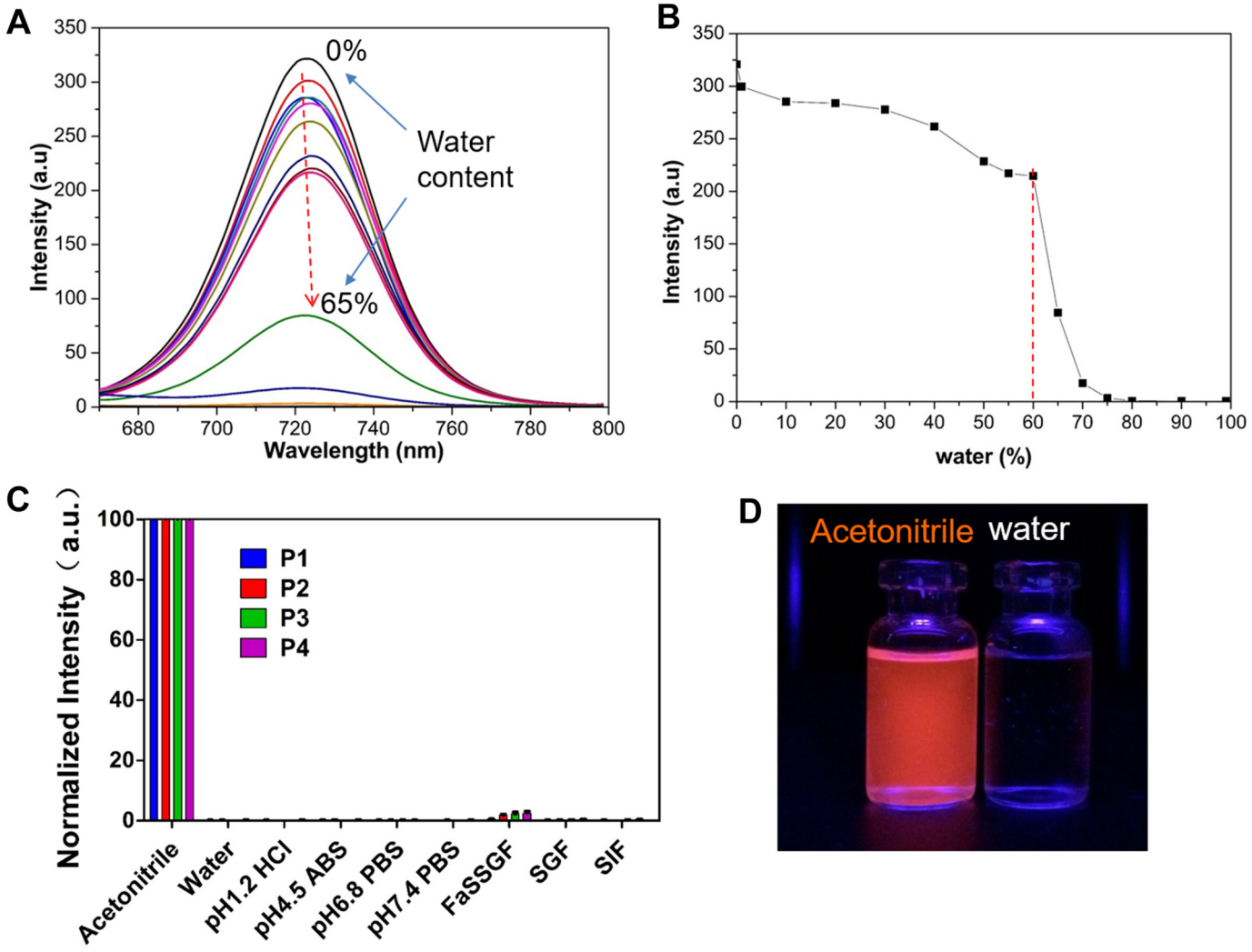

Fig. 6. Water-sensitivity of ACQ probes upon dilution from an organic solvent (acetonitrile) to aqueous media. A: fluorescence spectra of an aza-BODIPY dye (P2) as a function of water content; B: fluorescence *vs.* water content plot indicating the water-sensitivity threshold; C: fluorescence quenching upon dispersing the acetonitrile solution of ACQ probes (P1, P2, P3 and P4) into a 100% aqueous medium (ABS: acetate buffered saline; PBS: phosphate buffered saline; FaSSGF: fasted-state simulated gastric fluid; SGF: simulated gastric fluid; SIF: simulated intestinal fluid); D: fluorescent images of ACQ probes in acetonitrile (activated) *vs.* in water (quenched). Adapted from reference [72] with permission. Copyright 2015 Elsevier.

are performed as an alternative. For instance, the degradation of lipid nanoparticles by pancreatic lipases in the intestinal tract is an essential process to improve oral absorption. Measurements of the *in vivo* lipolysis process of lipid nanoparticles remain absent [18]. Although conventional probes may offer certain information on the *in vivo* translocation of labeled materials, they fail to monitor the degradation of nanocarriers because the fluorescence of probes do not change synchronously. The synchronicity between fluorescence quenching and degradation is essential to a more accurate monitoring of intact nanocarriers *in vivo* [97]. In a previous study, the fluorescence quenching of an ACQ dye was found to be synchronous to the degradation of SLNs [72]. The fluorescence intensities of P2-labeled SLNs during *in vitro* lipolysis were correlated well with the non-degraded SLNs, as reflected by the residual amount of NaOH that was used to neutralize the acid formed during lipolysis [72]. Conversely, the results obtained using DiR lacked synchronicity.

Only when the synchronicity between fluorescence quenching and the degradation of nanocarriers is established can the fluorescence be used to represent integral nanocarriers. Nevertheless, the soaking of the nanocarrier matrix in water and the diffusion of the dye molecules ahead of degradation will result in advanced fluorescence quenching and compromise the synchronicity.

3.4. Limitations

3.4.1. Inadaptability for hydrophilic nanocarriers

ACQ probes have been used in monitoring the *in vivo* fate of nanocarriers that are mainly composed of lipids or hydrophobic polymers [97,112,117,119]. Lipid-based nanocarriers such as SLNs, nanostructured lipid carriers (NLCs) and nanoemulsions have hydrophobic matrices that are able to solubilize hydrophobic dyes and maintain an emissive state. The high hydrophobicity of the nanocarrier matrices and their high affinity towards the probes prevent soaking of the matrices and advanced leakage of the probes ahead of degradation. Unfortunately, ACQ-based bioimaging is not applicable for hydrophilic nanocarriers because not only it is very difficult to encapsulate the dyes but also water tends to soak hydrophilic matrices very quickly (Fig. 8). Hydrophilic nanocarriers including nanogels, hydrophilic polymeric nanocarriers (e.g., chitosan nanoparticles) and mesoporous nanocarriers, as well as polyester nanocarriers of less hydrophobicity such as poly(lactic-co-glycolic acid) (PLGA) nanoparticles, fall within this category. As illustrated in Fig. 8, the hydrophilic matrix materials of these vehicles can be fully hydrated upon imbibition of water [118]. Following the swelling of the matrices, the ACQ payloads dissociate from the matrices and form aggregates immediately within the soaked

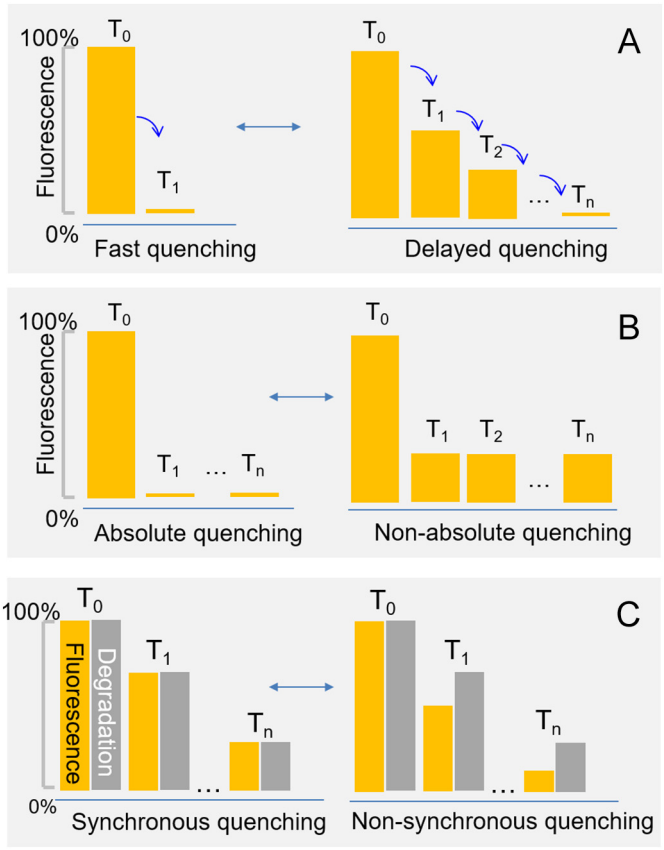

Fig. 7. Schematic presentation of fast *vs.* delayed (A), absolute *vs.* non-absolute (B) and synchronous *vs.* nonsynchronous (C) quenching. T_1, T_2, … and T_n refer to different measuring time. Panel A: the responsive rate of ACQ probes should be very fast with the original fluorescence (T_0) dropping abruptly from the highest (100%) to the lowest (0%) level before the first measurement time (T_1). Delayed quenching should be avoided because it takes longer time to achieve steady quenched state and compromises the real-time monitoring capacity. Panel B: when ACQ takes place, the original fluorescence (T_0) should drop to near 0% (T_1) and then keep steady for prolonged time durations (~T_n). If ACQ were non-absolute, the fluorescence would not drop to near zero, and the residual fluorescence would produce interference to the imaging. Panel C: In the synchronous quenching, the fluorescence quenching should keep pace with the degradation of the nanocarrier matrix, whereas in nonsynchronous quenching, the rate of fluorescence quenching differs from the degradation rate, reporting false information.

environment, leading to premature fluorescence quenching and the misreading of nanocarrier degradation.

3.4.2. Re-illumination due to repartitioning into hydrophobic constructs

ACQ probes form aggregates to cause fluorescent quenching *via* π-π stacking upon release along with the degradation of nanocarriers. Albeit not easily disassociated, the aggregates are able to repartition into hydrophobic domains in biological systems, including but not limited to biomembranes, the hydrophobic cavities of biomacromolecules and the hydrophobic cores of physiological micelles and fat tissues [95]. The redispersion of the aggregates into molecularly dispersed emissive states re-illuminates the probes. In addition, the aggregates can be disaggregated by some molecules of similar hydrophobicity, which can insert into the lattices of aggregates and dissociate them into monomers with the fluorescence turned on simultaneously (Fig. 9) [81]. The re-illumination brings about a pseudopositive interference in the tracking of nanocarriers. In oral delivery, quenched dyes may disaggregate and partition into mixed micelles formed by physiologically secreted surfactants (bile salts and phospholipids) to enable re-illumination [120]. The same was observed following *iv* administration, as well, because the lipid constituents in blood circulation dissociate the aggregates [95]. In addition to re-illumination due to the dissociation of fluorophore aggregates, the dyes may be transferred directly from an emissive state, as in the nanocarrier matrix, to hydrophobic domains. Both situations bring about interference to the monitoring of nanocarriers. Re-illumination represents one of the weaknesses in ACQ-based bioimaging and should by all means be curtailed to as little as possible. The previous findings indicated that only faint re-illumination was observed following gavage administration of a quenched dye control (P2) [72]. The re-illumination by blood is more significant than by gastrointestinal content [95]. It should be reminded that when there is less leakage of the probes, there will be less re-illumination, especially at the early stages of observation when the degradation of the nanocarrier matrix is not significant [95]. Since the repartitioning of hydrophobic fluorophores into hydrophobic regions is a natural process, it is very hard to eliminate the drawbacks of re-illumination. However, by optimization of fluorophore structures, the cohesion of quenched aggregates may be enhanced to prevent disaggregation and thereby re-illumination.

4. Application of ACQ-based bioimaging of nanocarriers

Based on the above discussion, it is concluded that the fluorescence emission could be used to represent integral drug nanocarriers [72,112]. The interference or artifacts due to free probes could be significantly reduced, making bioimaging more accurate [72,112]. Bearing this in mind, ACQ could be turned into a useful tool in not only unraveling the *in vivo* fate of drug nanocarriers but also various fields of bioscience and chemistry.

The most intriguing application of ACQ-based bioimaging is for the non-invasive real-time monitoring of drug nanocarriers *in vivo*. The information obtained *via* live imaging may tell the real-time distribution of the particles, rather than the drug payloads, carrier materials or probes. Altogether, with live imaging evidence collected by observing *ex vivo* tissues and/or by microscopic observation (e.g., CLSM), important conclusions can be drawn by highlighting the contribution of particles in the performance of drug nanocarriers. For instance, a scan of the cerebral tissues by live imaging clearly shows evidence to testify whether drug nanocarriers are able to cross the nose-to-brain barrier and reach the brain [121].

4.1. Oral delivery

The oral route is the most preferred route for drug delivery because of safety issues, convenience in storage and administration, availability of multiple dosage forms and good patient compliance. There is a growing trend of applying nanocarriers to enhance the oral bioavailability and efficacy of poorly water-soluble drugs and macromolecules [122–124]. However, the safety concerns incurred by nanocarriers and the ambiguity of the *in vivo* behaviors hindered the process of clinical translation [19,125]. Unraveling the *in vivo* fate of nanocarriers helps to elucidate the underlying mechanisms and to expedite formulation optimization. The *in vivo* fate of lipid nanoparticles, nanoemulsions, polymeric nanoparticles, polymeric micelles and nanocrystals have been investigated in animal models using ACQ-based bioimaging.

4.1.1. Lipid-based nanoparticles

Lipid-based nanoparticles (LBNs), including SLNs, NLCs and lipid-drug conjugates, are a category of important carriers for oral drug delivery. Since the main constituents of LBNs are lipids (triglycerides, diglycerides and monoglycerides) [126], LBNs are degradable by lipases in the GIT *via* a process of lipolysis [107,108]. To the contrary of previous studies on lipolysis done in simulated models, Hu et al. conducted real-time *in vivo* lipolysis of SLNs labeled by ACQ probes in nude mice for the first time [72]. Live imaging revealed the fast digestion of a majority of SLNs within 2 h following oral administration (Fig. 5B), and the high correlation between *in vivo* lipolysis, expressed as the integral fluorescence intensity based on a region-of-interest (ROI) method, and the *in vitro* data obtained by an alkaline compensation method validates the promise of the ACQ-based strategy [72]. In a follow-up study [112], Hu et al.

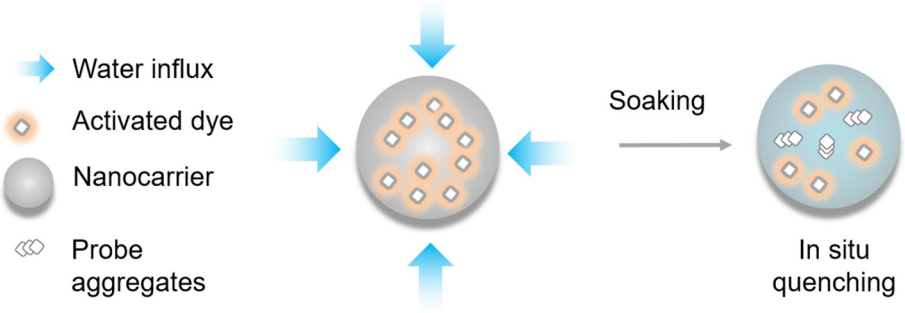

Fig. 8. Schematic presentation of premature quenching of fluorescence due to soaking of the hydrophilic matrix of nanocarriers. Soaking changes the nanocarrier matrix into an aqueous environment, leading to spontaneous aggregation of the probes and thereby premature fluorescence quenching that reports false signals of nanocarrier behaviors.

investigated the intragastrointestinal fate of SLNs in mice under fasted, fed, high-fat feeding and lipase-inhibition (by orlistat) conditions. There was a similar digestive trend observed by live imaging to the previous findings in nude mice. Nevertheless, Hu et al. took notice of the inherent limitations of the live imaging method due to limited penetration depth of fluorescence and went further to observe the dissected *ex vivo* tissues directly. The direct observation of the GIT *ex vivo* revealed unexpectedly long residence time of SLNs in the stomach for all groups, especially for the high-fat feeding and lipase-inhibition groups, which could be attributed to reduced gastric motility due to the prolonged presence of more lipids, according to the authors (Fig. 10) [112]. The stomach serves as a reservoir to supply SLNs to the small intestine, where the particles are degraded by lipases. High-fat feeding competitively consumes lipases, and pre-treatment with orlistat inhibits lipase activity, all leading to considerably reduced degradation of SLNs and prolonged residence time.

There are controversies with regard to the mechanisms behind the enhancement in oral absorption by LBNs. In addition to lipolysis [107,108], the hypothesis of absorption of integral LBNs surviving lipolysis has been proposed as well [127–129]. The evidence obtained by monitoring integral particles provides an explanation for the underlying mechanisms [72,112]. In spite of the proposed uptake and transport of SLNs by enteric epithelia as a means to enhance oral absorption [130,131], Hu et al.'s findings indicated no absorption and subsequent translocation of integral SLNs into circulation and then into tissues and organs [112]. However, in Ma et al.'s study, fluorescence

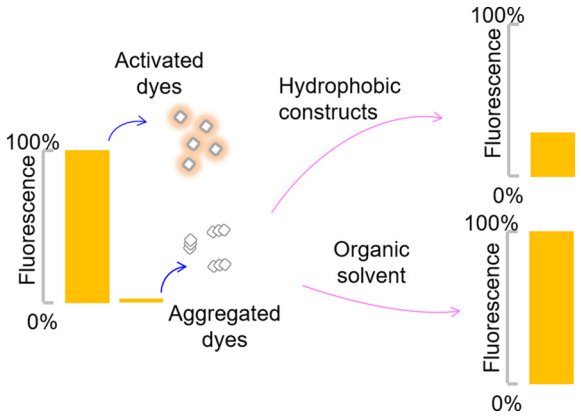

Fig. 9. Illustration of re-illumination of fluorescence due to repartitioning of aggregates into hydrophobic constructs. Activated dyes, as in the organic solvent, give full-scale fluorescence, whereas aggregated dyes, as in aqueous media, give almost no fluorescence at all. If the aggregated dyes are extracted with the organic solvent, then the fluorescence would recover to its original strength. Aggregated dyes are able to be redispersed molecularly and re-illuminated upon partitioning into hydrophobic constructs, such as micelles formed from surfactants. The degree of re-illumination varies according to the solubilizing capability of the hydrophobic constructs but is generally at a very low level due to the impediment encountered in overcoming the coherence of dye aggregates.

representing integral SLNs was observed in the livers after increasing the administered dose, raising the possibility of oral absorption of integral SLNs [119]. Further study indicated that a small amount of intact mixed micelles were observed to distribute mainly to the livers [120]. Therefore, they proposed that the transport of integral particles might be ascribed to mixed micelles, the products of lipolysis of SLNs. Nevertheless, the possibility of the absorption of integral LBNs should not be excluded.

Another ACQ probe (P4), with shorter emission wavelengths suitable for CLSM analysis, was used to study the intracellular fate of nanoparticles by CLSM. Both SLNs and mixed micelles exhibited enrichment on cell surfaces and significant cellular uptake, but no penetration across cell monolayers in both Caco-2 and Caco-2/HT-29-MTX (mimicking mucus secretion) cell models [112,119], strengthening the conclusion obtained *in vivo*.

4.1.2. Nanoemulsions

Nanoemulsions differ from SLNs only in the liquid lipids used in place of solid lipids [126,132]. Nanoemulsions have been broadly used as carriers for poorly water-soluble drugs due to their solubilization capacity, biocompatibility and absorption enhancement [133,134]. Xia et al. studied the gastrointestinal fate of nanoemulsions following protocols similar to those for SLNs but with an emphasis on the size effect [97]. Results similar to SLNs were observed with regard to lipolysis both *in vitro* and *in vivo*. Live imaging demonstrated a size dependency for both digestion and epithelial uptake of nanoemulsions [97], which complies with reports by other groups using different methods [135,136]. Smaller nanoemulsions (80 nm) showed enhanced bioadhesion with intestinal epithelia (Fig. 11A & B) and pervasive distribution into enterocytes and basolateral tissues, while bigger ones (550, 1000 nm) primarily adhered to but not across villi surfaces [97] (Fig. 11C). Once again, the distribution of a fraction of integral nanoemulsions into the livers and lungs was observed one hour after administration, with an explanation of transport *via* the lymphatic pathway [97].

4.1.3. Glucan microparticles

Glucan microparticles (GMs), also known as yeast cell wall particles, are prepared from *Saccharomyces cerevisiae* (Baker's yeast) and possess a hollow ellipsoid structure with porous shells and a diameter of 2-4 μm. Their primary component is β-1,3-D-glucan, a ligand of CR3 and dectin-1 receptors expressing on phagocytes including M cells, macrophages, neutrophils and dendritic cells [137]. GMs have been employed to deliver vaccines, siRNA and insulin [124,138,139] orally by a generally recognized mechanism of uptake by M cells located in intestinal Peyer's patches and subsequent transport *via* the lymphatic route [140,141]. The relatively large size of GMs renders them easily recognizable in biological tissues with the aid of imaging tools. Following labeling with ACQ probes by first dissolving in melted stearin and then incorporating into the inner cores of GMs, GMs were observed distributing to the basolateral side of ileum through Peyer's patches and were recovered

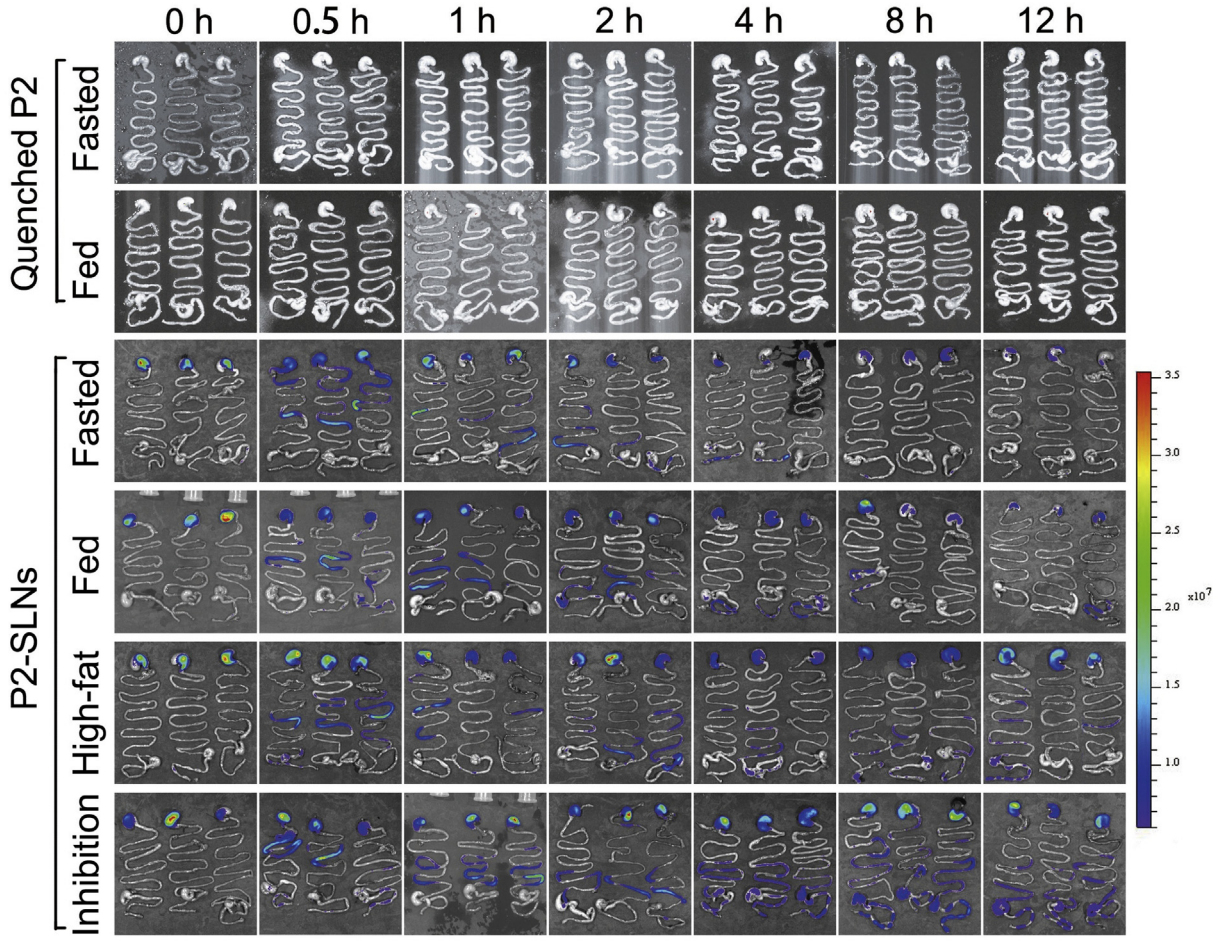

Fig. 10. Images of *ex vivo* tissues indicate the transport of SLNs in the GIT under fed, fasted, high-fat and lipase-inhibition (by orlistat) states. From top to bottom in each image panel: stomach, small intestine and colon. The fluorescence represents integral SLNs. The comparison between groups and different sampling time points reveals the effect of various factors on the gastrointestinal fate of SLNs. The quenched P2 dye control does not give fluorescent signals, indicating negligible interference owing to re-illumination. Adapted from [112] with permission. Copyright 2016 Royal Society of Chemistry.

in the liver, spleen and lung 12 h after administration (Fig. 12A) [96]. Each dot in the CLSM images represents one GM, and the distribution of the fluorescence dots outlines the follicle-associate epithelia (Fig. 12B) [96], also named as the "dome trap" after Qi et al. [141] Further study in Caco-2/Raji B co-culture models (mimicking M cell function) revealed "voracious" engulfing of GMs by macrophages (J774A.1) located beneath the monolayers (Fig. 12C), strengthening the lymphatic route as a pathway for GM absorption [96]. More interestingly, most GMs captured by macrophages were entrapped for extended times, implying easy phagocytosis but hard exocytosis in the dome trap [96].

4.1.4. Polymeric nanoparticles

Polymeric nanoparticles (PNs) were introduced into oral drug delivery because of their protective effect of labile biomacromolecules against harsh environments and their increased uptake by intestinal epithelia [142,143]. The labile entities are not meant to be released in the GIT because the released biomacromolecules would be destroyed quickly by gastric acid, enzymes and bile salts. There must be alternative pathways for oral absorption, if the drugs do not release at all. To date, no evidence, qualitative or quantitative, is available to clarify the mechanisms of the oral absorption of nanocarriers. In He et al.'s study, the size effect on the translocation of PCL nanoparticles was investigated using the ACQ tools [144]. Smaller nanoparticles (< 200 nm) were integrally transported across the intestinal epithelia and accumulated mainly in the livers, whereas the particles larger than 600 nm could not be absorbed, or could be absorbed only in a minute amount, as integral particles into circulation. Both the M cells and enterocytes contribute to the transport of PCL nanoparticles (50 nm) [144].

4.1.5. Nanocrystals

Solid dosage forms are primarily comprised of drug crystals whose dissolution is one of the rate-limiting steps to oral bioavailability. The development of nanocrystals creates opportunities for the bioavailability enhancement of poorly water-soluble drugs due to an improved solubility and dissolution rate [145]. Although it is very easy to determine the dissolution *in vitro*, *in vivo* dissolution has not yet been well studied. Studies with autofluorescence drugs, such as coumarin 6, have provided limited information on their *in vivo* behaviors [146,147], and it is difficult to split the fluorescence into that of drug crystals and that of dissolved drug molecules, not to mention the availability of limited number of autofluorescent drugs. Inspired by the hybrid crystallization process, fluorophores have been embedded into crystal lattices to form hybrid fluorescent nanocrystals [31]. A few tens of fluorophores (fluorescein, rhodamine B, DiD, DiR, Cy5, etc.) have been employed to hybridize drug nanocrystals for the non-invasive and real-time tracking of their biological fate [30,42]. To overcome the drawbacks of the lack of discrimination between dissolved and crystal forms, ACQ probes have been used to replace conventional fluorophores to hybridize and illuminate nanocrystals [106]. Using cyclosporine A and quercetin as model drugs, live imaging results indicated that drug crystals could survive in the GIT for 12-18 h and that a small fraction of drug nanocrystals could be absorbed, in particulate form, into systemic circulation and

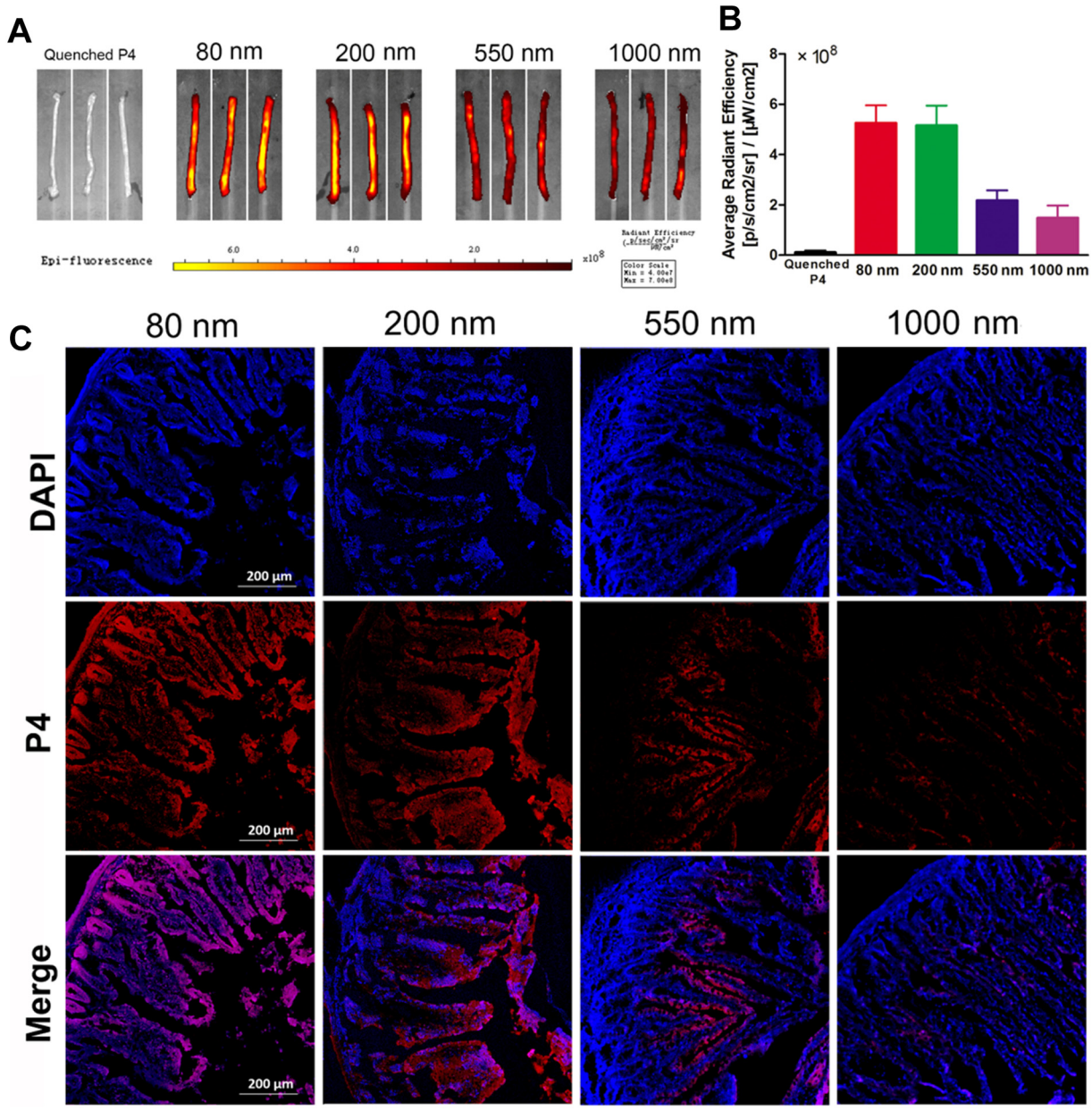

Fig. 11. Live imaging (A) and fluorescent quantification (B) of the bioadsorption of nanoemulsions following one-direction *in situ* perfusion; CLSM images of frozen section of jejunum segments (C). P4 (red) and DAPI (blue) signals stand for nanoemulsions and cell nuclei, respectively; colocalization of the signals (pink) highlights the infiltration of nanoemulsions (especially 80 nm), into basolateral tissues. Reprinted with permission from [97]. Copyright 2017American Chemical Society.

subsequently distributed into the livers and lungs [106,148]. For further reading, please refer to another review article in this issue.

4.2. Intravenous delivery

The successful marketing of several products (Doxil®, Abraxane® and Genexol-PM®) has evoked enthusiasm for the research and development of nanomedicines, especially for cancer chemotherapy. It is of critical importance to depict the *in vivo* fate of nanocarriers for a better understanding of their pharmacological and toxicological activities [118,149].

4.2.1. Polymeric nanoparticles

Meng et al. investigated the biodistribution of intravenously administered PLGA nanoparticles quantitatively by taking advantage of the ACQ property of the near-infrared fluorophore DiR [69]. The lack of fluorescence linearity led the authors to question the reliability of the fluorescence quantification [69]. Meng et al.'s work implied that the combination of a conventional fluorophore (DiR) and PLGA nanoparticles with water-penetrable matrices was not a good choice. DiR is subject to concentration quenching but is not generally regarded as an absolute-quenching probe. The high background interference due to incomplete quenching should not be neglected, and this might be the issue that complicates the fluorescent quantification in Meng et al.'s work [69]. In addition, ACQ probes are not suitable for nanocarriers with inadequate hydrophobicity (including PLGA nanoparticles) because of the premature quenching of the probes caused by soaking of the nanocarriers, as discussed in Part *3.3.1*. The use of nanocarriers with more hydrophobic matrices and fluorophores with absolute ACQ properties would add strength to their findings.

Taking advantage of the fast and absolute quenching features of an aza-BODIPY dye (P2), He et al. reassessed the long-circulating effect using paclitaxel-loaded PCL nanoparticles as a model [117]. The kinetic profiles of the particles reaffirmed long circulation by PEGylation, but

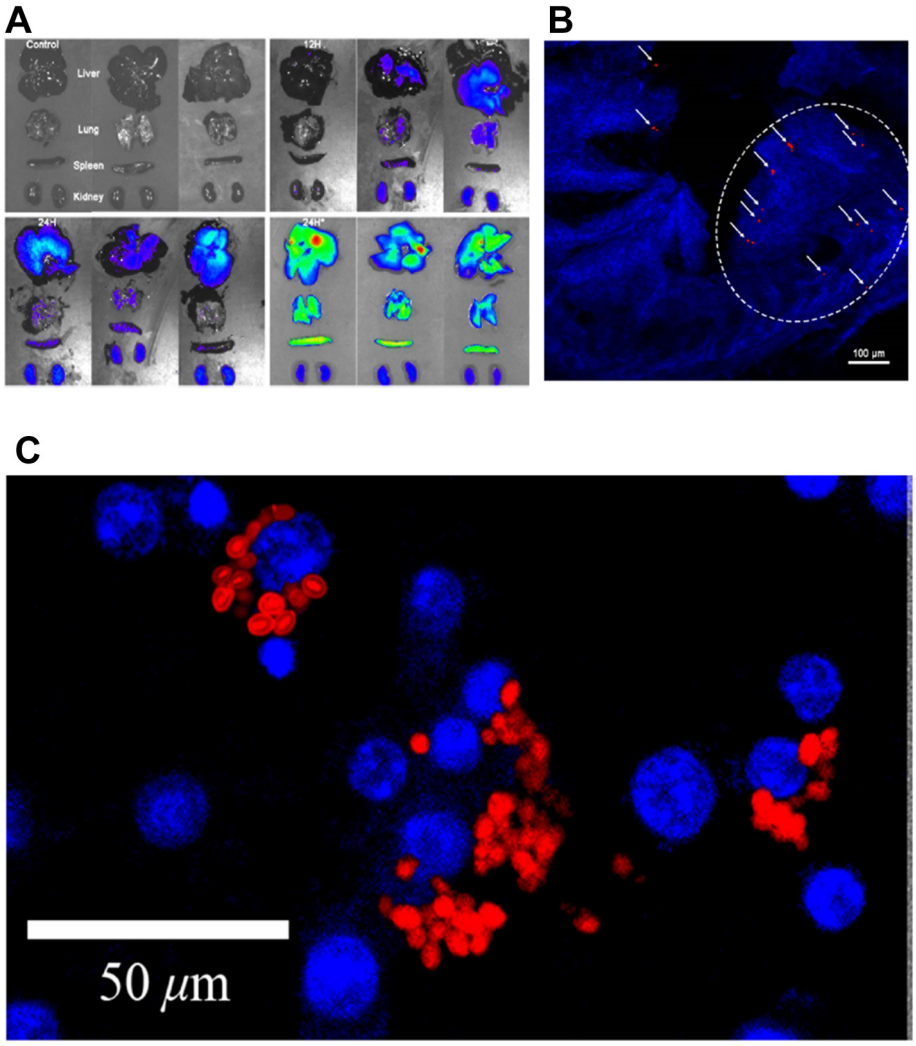

Fig. 12. Uptake of GMs (red dots) by follicle-associated epithelia outlines the frame of Peyer's patches or "dome traps" (A). GMs are transported to various organs via circulation following oral administration (from top to bottom in organ panels: liver, lung, spleen and kidney) (B). Voracious engulfing of GMS (red) by macrophages *via* phagocytosis was recorded using CLSM (C). Adapted with permission from [96]. Copyright 2016 Royal Society of Chemistry.

the authors pointed out that the observed long circulation was not as long as generally perceived, with blood levels dropping to below 20% within 2-4 h (Fig. 13A & B). A comparison between the kinetics of the particles and paclitaxel (Fig. 13C & D) revealed diverged profiles from the beginning of administration (Fig. 13E). The drug might have leaked very quickly from the nanocarriers into blood, raising a very interesting argument that only the vehicles, rather than the drug, are delivered to target sites. He et al.'s findings reveal the drawbacks of conventional protocols in monitoring drug levels for the investigation of nanoparticle kinetics.

4.2.2. Polymeric micelles

Polymeric micelles (PMs) are self-assembled core-shell nanocarriers formed by block copolymers. In the wake of the recent marketing of paclitaxel PMs product (Genexol-PM®) in Korea, PMs have drawn intensive attention as delivery carriers for poorly water-soluble drugs [150,151]. Despite its success, the *in vivo* fate of PMs following intravenous administration has yet to be elucidated [152,153]. One common viewpoint believes that the micellar structures dissociate rapidly once entering the blood stream due to an instantaneous dilution to a concentration below the critical micelle concentration (CMC) of the copolymers [154,155]. Paradoxically, PMs have been employed as common vehicles for drug delivery, apparently against the above hypothesis of structural dissociation *in vivo* [156,157]. What actually happens to PMs in circulation remains a mystery, and the exploration of the *in vivo* fate of PMs is of high translational significance, both clinically and industrially. He et al. tracked the distribution of integral PM particles by labeling with ACQ probes [95]. The imaging evidence indicated that the level of integral PMs in blood, as well as that in various organs such as the livers, lungs, spleen and kidneys, decreased gradually and then remained for several hours [95]. It is fair to say PMs are robust enough to withstand the detrimental physiological milieu. It seems that PMs may not be as fragile as generally perceived for micellar structures *in vivo*.

4.2.3. Nanocrystals

The hybridized nanocrystal technology developed by Tonglei Li and coworkers is a workable approach for visualization of the *in vivo* fate of drug nanocrystals [42]. The fortification with environment-responsive probes strengthen the power of this technology [106]. Gao et al. employed the AIE probe, tetraphenylethene (TPE), to explore the kinetic process of the dissolution of nanocrystals in cancer cells, and the results suggested that drug nanocrystals were taken up directly by the cells and subsequently dissolved in the cytoplasm [158]. Unfortunately, TPE is not suitable for *in vivo* study because of its short emissive wavelengths. Wang et al. labeled curcumin nanocrystals with a near-infrared ACQ probe (P2) to visualize the biodistribution of nanocrystals following intravenous administration [159]. A large fraction of curcumin

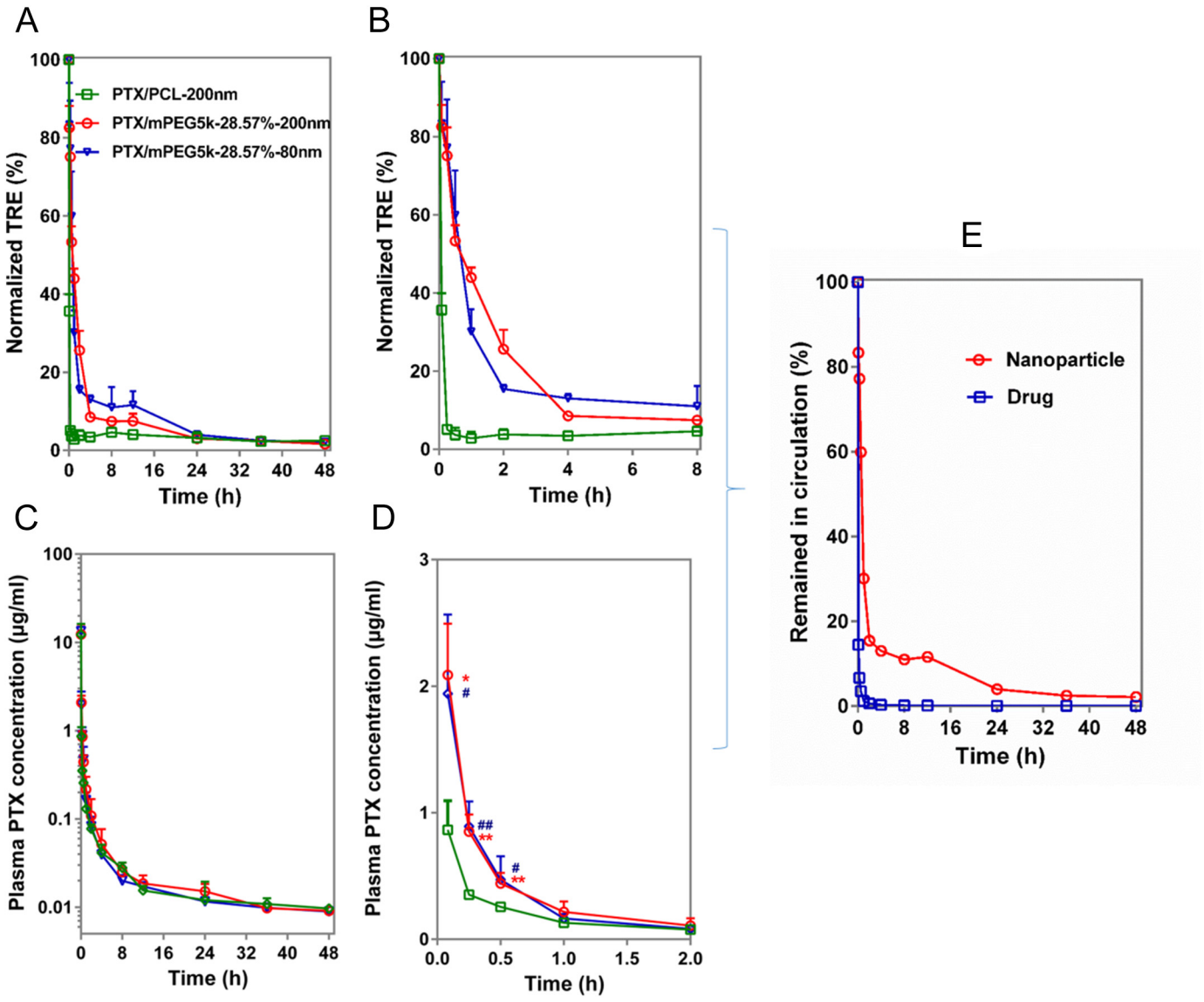

Fig. 13. The kinetic profiles in blood of paclitaxel-loaded PCL nanoparticles of different sizes and with different degrees of PEG coating. A: nanoparticles *vs.* time plot, as measured by monitoring integral particles using the ACQ-based strategy; B: an enlargement of plot A within 0-8 h; C: paclitaxel *vs.* time plot; D: an enlargement of plot B within 0-2 h; E: an example showing the disparity between the kinetics of the particles and the drug paclitaxel following normalization of the initial blood levels to 100%. Adapted with permission from [117]. Copyright 2017 Royal Society of Chemistry.

nanocrystals were cleared from the blood rapidly and distributed to the livers and lungs, but a small fraction circulated in the blood for as long as 48 h due to a surface coating of poloxamer 188. These findings are reminiscent of the potential for local toxicity in various organs and tissues as a result of the accumulation of drug nanocrystals, especially when the active ingredients are highly toxic.

4.3. Transdermal delivery

Nanoformulations of nanoemulsions, liposomes, lipid nanoparticles and micelles are playing an increasingly important role in the enhancement of drug penetration into and across skin [160,161]. However, the contribution of nanocarriers remains largely unknown, despite some reports suggesting penetration of integral vehicles across the multiple layers of intact skin. This predicament is ascribed to the lack of reliable approaches to track the nanocarriers. Given the characteristics of ACQ probes, the mechanisms of transdermal delivery of nanoemulsions was partly elucidated based on tracking the translocation of intact nanoemulsions. The 80-nm nanoemulsions could integrally diffuse into but not cross the viable epidermis [162]. By contrast, the intact nanoemulsions could migrate to as deep as 588 μm into the dermis along the hair follicle canals [162]. In addition, the released cargos could diffuse into the surrounding dermal tissues, and intact nanoemulsions could be taken up by antigen-presenting cells located in the epidermis or hair follicles [162].

4.4. Intranasal delivery

The nose-to-brain pathway has emerged as a shortcut for cerebral drug delivery, and previous results have suggested that nanocarriers play an important role [163–165]. However, the exact fate of the nanocarriers and payloads through the nose-to-brain pathway remains unclear. It is urgent to elucidate whether and to what extent the nanocarriers are able to be translocated to the cerebral regions. An understanding of this issue helps to make wise use of the nanocarriers when designing intranasal nanoformulations. ACQ probes (P2 and P4) were successfully applied to illuminate nanoemulsions during intranasal delivery. The nasal residence time of the nanoemulsions with small particle sizes (100 nm) is significantly longer than that of the larger ones, and intact nanoemulsions could be found in the trigeminal nerve

and olfactory bulb but not in the brain [121]. In contrast, a significant amount of payload (coumarin 6) signals were found along the nose-to-brain passage, finally reaching the brain [121]. The authors drew the conclusion that nanoparticles could hardly penetrate into the brain along the nose-to-brain pathway, whereas a fraction of the cargo entered the brain after release from the nanocarriers.

4.5. Ocular delivery

Owing to the unique physiological structure of the eyes, ocular drug delivery remains a challenge, especially for the posterior segment [166,167]. It is more challenging to treat posterior disease by non-invasive means, such as using eyedrops [168]. Recently, novel formulations based on microcarriers and nanocarriers have been investigated for various purposes, such as sustained release and enhanced penetration [169,170]. It would be very interesting to determine how deep and by which route nanocarriers could penetrate into various ocular tissues. In Wan et al.'s study [171], after administration *via* the intravitreal route, the levels of ACQ probe-labeled PCL nanoparticles found in ocular tissues were higher than levels in both the retrobulbar and the subtenon routes. In addition, intravitreal injection is more efficient in the delivery of intact nanoparticles to the retina than periocular administration. The nanoparticles are eliminated from the retina very fast after intravitreal administration; however, the drug molecules are released gradually and able to permeate into the retina through the transscleral pathway [171].

4.6. Turn-on ACQ template nanoparticles

In a recent study by Cheung and O'Shea [114], the ACQ effect was employed reversely to label drug crystals efficiently and track the subcellular translocation of the nanoparticles. Although this strategy differs from the main topic of this article, we would like to make a brief introduction to remind the readers of the different ways to use the ACQ rationale.

Direct labeling by the adsorption of the fluorophore molecules onto crystal surfaces failed because the fluorophores tended to form aggregates, rather than adsorb onto surfaces, due to the ACQ effect. In this study, aggregates of a fluorophore from the BODIPY family, NIR-AZA, were employed as templates to form non-emissive nanoparticles coated with poloxamer 188 *via* self-assembling. The nanoparticles are dark off in aqueous solution but turned on upon transformation into micelles (Fig. 14A) or upon contact with hydrophobic surfaces or interfaces. Redispersion of the quenched aggregates in the form of nanoparticles illuminates the vehicles or surfaces stained by the fluorophore monomers. As shown in Fig. 14B, the drug (ibuprofen) crystals could be illuminated following cultivation with nonfluorescent NIR-AZA nanoparticles. Using the nanoparticles as representative delivery vehicles and NIR-AZA as a representative hydrophobic drug, the cellular uptake and release process could be visualized in real time as the fluorophore was continuously released while staining various cell components (Fig. 14C & D).

4.7. Others

In the most recent study by Huang et al. [172], SLNs were labeled by an ACQ dye (P4) and were monitored for deposition in the lung. Nevertheless, one should be careful to use ACQ dyes in nanocarriers for pulmonary delivery because the lung is rich in physiological surfactants that might cause re-illumination of quenched probes and bring about interference.

The power of the ACQ rationale has been extended beyond application in the exploration of the biological fate of nanocarriers. In Lv et al.'s work, ACQ probes were used to visually validate the measurement of entrapment efficiency [173]. The crucial step in the measurement was the separation of the nanocarrier-associated from the non-associated drugs. The illumination of the nanocarriers made it probable to visualize whether the separating operation was efficient. Their results confirmed that ultrafiltration was the optimal method for separation, whereas centrifugation was very poor in separation even under extreme centrifugation forces [173].

5. Conclusions and perspectives

The demand for understanding the *in vivo* fate and cellular pharmacokinetics of nanocarriers calls for more accurate monitoring of nanocarriers. One of the most challenging obstacles is the difficulty in discriminating nanocarriers from bulk signals comprised of a mixed signals of both nanocarriers and free probes. The emergence of environment-responsive probes provides a potential solution to this challenge. Different from environment-responsive probes based on FRET and AIE, ACQ probes glow when embedded in the matrices of nanocarriers but quench immediately and absolutely when released into the ambient aqueous environment upon the degradation of the nanocarriers. ACQ, a common unfavorable effect with fluorescent bioimaging, is being turned into a useful tool towards more accurate bioimaging of nanocarriers.

When ACQ probes are molecularly dispersed in a favorable solvent or in the matrices of nanocarriers, they are dispersed in an emissive state and can be used to label nanocarriers. However, the probes form aggregates and quench instantly with fluorescence down to zero due to the ACQ effect when they are released upon degradation of nanocarriers. The interference due to free probes can be substantially reduced. The fluorescence observed during bioimaging represents integral nanocarriers. Based on this rationale, the *in vivo* fates of various nanocarriers (SLNs, nanoemulsions, PMs, PNs and nanocrystals) *via* various administrative routes (oral, intravenous, transdermal, intranasal, ocular and pulmonary) have been investigated with new evidence justifying the conventional knowledge on the acting mechanisms of drug nanocarriers.

The ACQ-based bioimaging strategy is not without drawbacks because ACQ is a natural process that is subject to the influence of natural factors. It is not suitable for hydrophilic nanocarriers because the hydrophilic matrices could be easily soaked, immediately leading to ACQ of the embedded fluorophores. Re-illumination due to disaggregation and repartitioning of the probe molecules into physiological hydrophobic domains brings about potential interference. To date, the observation of fluorescence re-illumination following administration of prequenched ACQ probes (an aggregate form treated as a control) indicates mild re-illumination within limited observation windows, and the re-illumination generated is believed not to pose significance interference to the bioimaging of nanocarriers.

ACQ-based bioimaging has been proven to be a universal tool to explore the *in vivo* fate and cellular pharmacokinetics of versatile drug nanocarriers *via* various administrative routes. In addition to the nanocarriers and the administrative routes mentioned in this article, the ACQ-based strategy may be promoted for use in a wider spectrum of nanocarriers *via* a wider variety of administrative routes. By tracking the translocation of the particles, the behaviors of nanocarriers themselves, as well as their interactions with the biological environment, can be made clearer. The quantitative correlation between fluorescence and the amount of nanocarriers creates opportunities for the exploration of particokinetics. If both the loaded drugs and the construction materials of the nanocarriers are monitored together with the particles, a panorama of the spatiotemporal fate of drug-loaded nanocarriers could be depicted, revealing important information for the elucidation of underlying mechanisms such as *in vivo* drug release and degradation kinetics.

Based on the "on→off" signal switching mode, ACQ probes are expected to find applications in the wider field of bioscience and chemistry. This tool would become very powerful if used appropriately. Assisted by live imaging equipment, ACQ probes-labeled nanocarriers

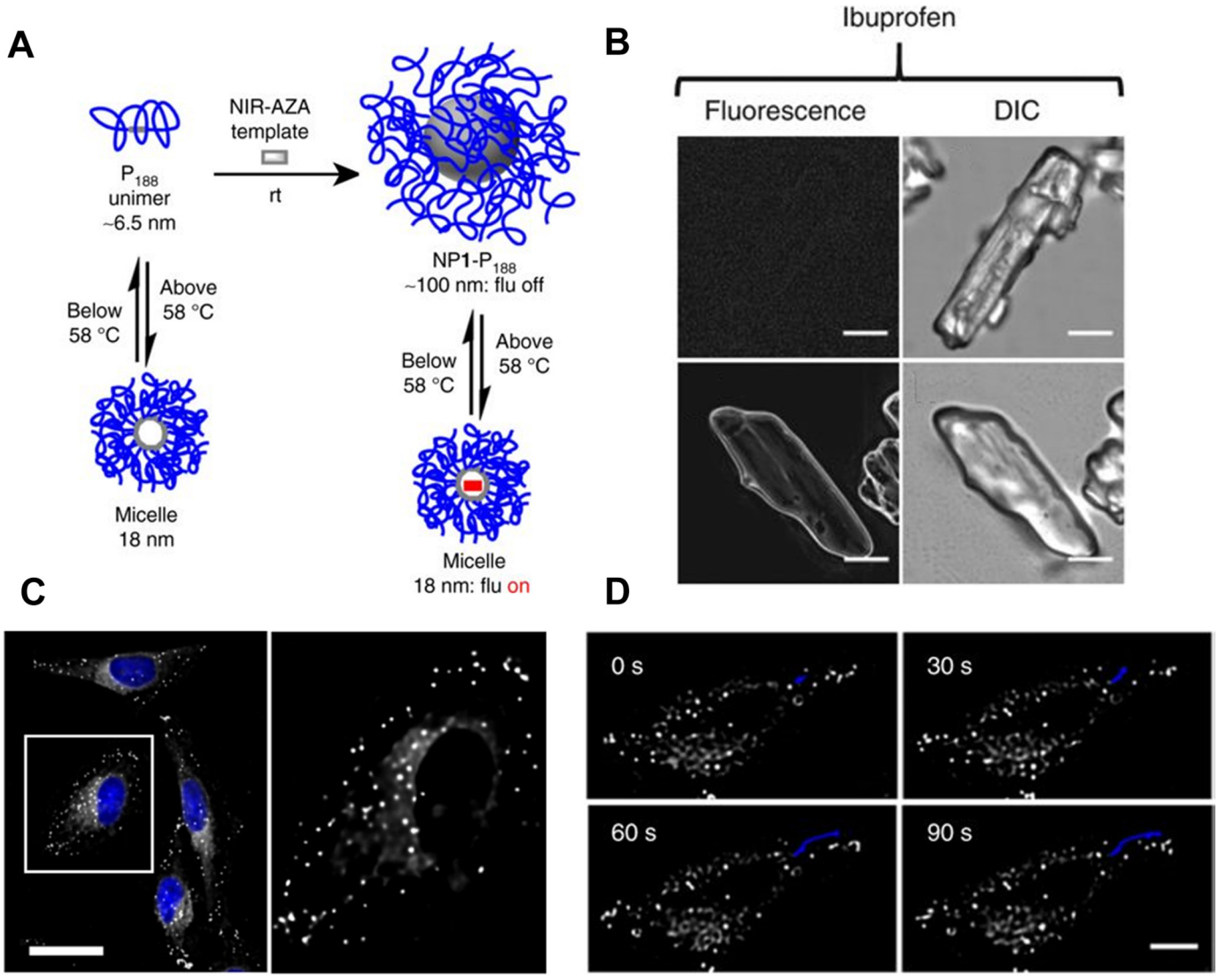

Fig. 14. Quenched NIR-AZA template nanoparticles are used to stain hydrophobic drug crystals and cellular membranes. A: The poloxamer 188-coated NIR-AZA template nanoparticles (~100 nm) are dark but can be turned on above the critical micelle temperature of poloxamer 188 (58°C) owing to the formation of poloxamer 188 micelles (~18 nm); B: the cultivation of the template nanoparticles with drug (ibuprofen) crystals illuminates the crystal surfaces; C: images of multiple Hela-Kyoto cells and a single cell expansion following incubation with the template nanoparticles for 2 h reveals the traces of cellular uptake and trafficking (scale bar: 20μm); D: the blue line indicates the track of a single vesicle over 90 s in a single cell at 20 min following cultivation with the template nanoparticles (scale bar: 20μm). Adapted with permission from [114]. Copyright 2017 Nature.

could be identified as particles in various separation operations, and the evidence obtained could be used to testify the efficiency of the separation. The validation of the entrapment efficiency of drug-loaded nanocarriers, as described in this article is a preliminary and exemplary application of this regard. More applications in the field of colloidal and surface science are expected.

Although fluorescence re-illumination was observed not to cause significant interference during bioimaging, the removal of all re-illumination is expected. However, this is not an easy task because the re-illumination due to partition to hydrophobic domains is a natural process. To address the drawbacks of fluorescence re-illumination, next-step work is directed towards reduction of the re-illumination by optimization of the molecular structures of probes to increase the coherency of the aggregates and reduce disaggregation. Regardless, the ACQ-based approach is better than conventional bioimaging approaches using non-environment-responsive probes.

Moreover, the conceptualization of the basic thinking behind the identification of integral nanocarriers as derived from ACQ-based bioimaging might be proven to be of even more importance. The accurate bioimaging of drug nanocarriers can be achieved by versatile strategies or probes beyond the use of ACQ probes. Environment-responsive probes, including FRET fluorophores that have shown some potential, are expected to play a more active role towards this direction.

Declarations of interest

None.

Acknowledgements

This work is financially supported by National Natural Science Foundation of China (81573363, 81872815, 81872826 and 81690263), Shanghai Municipal Commission of Science and Technology (19XD1400300 and 18410741800) and National Key Basic Research Program (2015CB931800).

References

[1] K. Park, Drug delivery of the future: Chasing the invisible gorilla, J. Control. Release 240 (2016) 2–8.

[2] S. Chen, X.J. Liang, Nanobiotechnology and nanomedicine: small change brings big difference, Sci. China Life Sci. 61 (2018) 371–372.
[3] M.L. Etheridge, S.A. Campbell, A.G. Erdman, C.L. Haynes, S.M. Wolf, J. McCullough, The big picture on nanomedicine: the state of investigational and approved nanomedicine products, Nanomedicine 9 (2013) 1–14.
[4] S. Aftab, A. Shah, A. Nadhman, S. Kurbanoglu, S. Aysil Ozkan, D.D. Dionysiou, S.S. Shukla, T.M. Aminabhavi, Nanomedicine: An effective tool in cancer therapy, Int. J. Pharm. 540 (2018) 132–149.
[5] S. Tran, P.J. DeGiovanni, B. Piel, P. Rai, Cancer nanomedicine: a review of recent success in drug delivery, Clin. Transl. Med. 6 (2017) 44.
[6] J. Shi, P.W. Kantoff, R. Wooster, O.C. Farokhzad, Cancer nanomedicine: progress, challenges and opportunities, Nat. Rev. Cancer 17 (2017) 20–37.
[7] S.A. El-Zahaby, Y.S.R. Elnaggar, O.Y. Abdallah, Reviewing two decades of nanomedicine implementations in targeted treatment and diagnosis of pancreatic cancer: An emphasis on state of art, J. Control. Release 293 (2019) 21–35.
[8] K. Greish, A. Mathur, M. Bakhiet, S. Taurin, Nanomedicine: is it lost in translation? Ther. Deliv. 9 (2018) 269–285.
[9] A. Wicki, D. Witzigmann, V. Balasubramanian, J. Huwyler, Nanomedicine in cancer therapy: challenges, opportunities, and clinical applications, J. Control. Release 200 (2015) 138–157.
[10] J.B. Coty, C. Vauthier, Characterization of nanomedicines: A reflection on a field under construction needed for clinical translation success, J. Control. Release 275 (2018) 254–268.
[11] M. Faria, M. Bjornmalm, K.J. Thurecht, S.J. Kent, R.G. Parton, M. Kavallaris, A.P.R. Johnston, J.J. Gooding, S.R. Corrie, B.J. Boyd, P. Thordarson, A.K. Whittaker, M.M. Stevens, C.A. Prestidge, C.J.H. Porter, W.J. Parak, T.P. Davis, E.J. Crampin, F. Caruso, Minimum information reporting in bio-nano experimental literature, Nat. Nanotechnol. 13 (2018) 777–785.
[12] E.B. Manaia, M.P. Abucafy, B.G. Chiari-Andreo, B.L. Silva, J.A. Oshiro Junior, L.A. Chiavacci, Physicochemical characterization of drug nanocarriers, Int. J. Nanomedicine 12 (2017) 4991–5011.
[13] K. Park, Facing the truth about nanotechnology in drug delivery, ACS Nano 7 (2013) 7442–7447.
[14] N. Feliu, D. Docter, M. Heine, P. Del Pino, S. Ashraf, J. Kolosnjaj-Tabi, P. Macchiarini, P. Nielsen, D. Alloyeau, F. Gazeau, R.H. Stauber, W.J. Parak, In vivo degeneration and the fate of inorganic nanoparticles, Chem. Soc. Rev. 45 (2016) 2440–2457.
[15] M. Zhu, G. Nie, H. Meng, T. Xia, A. Nel, Y. Zhao, Physicochemical properties determine nanomaterial cellular uptake, transport, and fate, Acc. Chem. Res. 46 (2013) 622–631.
[16] B. Wang, X. He, Z. Zhang, Y. Zhao, W. Feng, Metabolism of nanomaterials in vivo: blood circulation and organ clearance, Acc. Chem. Res. 46 (2013) 761–769.
[17] Y. Jin, D. Kim, H. Roh, S. Kim, S. Hussain, J. Kang, C.G. Pack, J.K. Kim, S.J. Myung, E. Ruoslahti, M.J. Sailor, S.C. Kim, J. Joo, Tracking the fate of porous silicon nanoparticles delivering a peptide payload by intrinsic photoluminescence lifetime, Adv. Mater. 30 (2018), e1802878.
[18] J. Qi, J. Zhuang, Y. Lu, X. Dong, W. Zhao, W. Wu, In vivo fate of lipid-based nanoparticles, Drug Discov. Today 22 (2017) 166–172.
[19] X. Hu, X. Dong, Y. Lu, J. Qi, W. Zhao, W. Wu, Bioimaging of nanoparticles: the crucial role of discriminating nanoparticles from free probes, Drug Discov. Today 22 (2017) 382–387.
[20] A.L. Laine, J. Gravier, M. Henry, L. Sancey, J. Bejaud, E. Pancani, M. Wiber, I. Texier, J.L. Coll, J.P. Benoit, C. Passirani, Conventional versus stealth lipid nanoparticles: formulation and in vivo fate prediction through FRET monitoring, J. Control. Release 188 (2014) 1–8.
[21] W. Xiao, H. Gao, The impact of protein corona on the behavior and targeting capability of nanoparticle-based delivery system, Int. J. Pharm. 552 (2018) 328–339.
[22] N. Bertrand, P. Grenier, M. Mahmoudi, E.M. Lima, E.A. Appel, F. Dormont, J.M. Lim, R. Karnik, R. Langer, O.C. Farokhzad, Mechanistic understanding of in vivo protein corona formation on polymeric nanoparticles and impact on pharmacokinetics, Nat. Commun. 8 (2017) 777.
[23] X. He, Y. Ma, M. Li, P. Zhang, Y. Li, Z. Zhang, Quantifying and imaging engineered nanomaterials in vivo: challenges and techniques, Small 9 (2013) 1482–1491.
[24] K. Stojanov, I.S. Zuhorn, R.A. Dierckx, E.F. de Vries, Imaging of cells and nanoparticles: implications for drug delivery to the brain, Pharm. Res. 29 (2012) 3213–3234.
[25] S.H. Hong, Y. Sun, C. Tang, K. Cheng, R. Zhang, Q. Fan, L. Xu, D. Huang, A. Zhao, Z. Cheng, Chelator-free and biocompatible melanin nanoplatform with facile-loading gadolinium and copper-64 for bioimaging, Bioconjug. Chem. 28 (2017) 1925–1930.
[26] M. Wang, Y. Qu, D. Hu, L. Chen, K. Shi, Y. Jia, Y. Yi, Q. Wei, T. Niu, Z. Qian, Methotrexate-loaded biodegradable polymeric micelles for lymphoma therapy, Int. J. Pharm. S0378-5173 (2018) 30935–30939.
[27] L. Wang, M. Liu, Y. Chen, Carbon dots and terbium co-enhanced fluorescence of europium nanoparticles for cell imaging, J. Biomed. Nanotechnol. 14 (2018) 1898–1905.
[28] S. Stremersch, T. Brans, K. Braeckmans, S. De Smedt, K. Raemdonck, Nucleic acid loading and fluorescent labeling of isolated extracellular vesicles requires adequate purification, Int. J. Pharm. 548 (2018) 783–792.
[29] F. Deng, H. Zhang, X. Wang, Y. Zhang, H. Hu, S. Song, W. Dai, B. He, Y. Zheng, X. Wang, Q. Zhang, Transmembrane pathways and mechanisms of rod-like paclitaxel nanocrystals through MDCK polarized monolayer, ACS Appl. Mater. Interfaces 9 (2017) 5803–5816.
[30] C.P. Hollis, H.L. Weiss, B.M. Evers, R.A. Gemeinhart, T. Li, In vivo investigation of hybrid Paclitaxel nanocrystals with dual fluorescent probes for cancer theranostics, Pharm. Res. 31 (2014) 1450–1459.
[31] R. Zhao, C.P. Hollis, H. Zhang, L. Sun, R.A. Gemeinhart, T. Li, Hybrid nanocrystals: achieving concurrent therapeutic and bioimaging functionalities toward solid tumors, Mol. Pharm. 8 (2011) 1985–1991.
[32] Y.F. Wang, T. Zhang, X.J. Liang, Aggregation-induced emission: lighting up cells, revealing life! Small 12 (2016) 6451–6477.
[33] T. Liu, Z. Liu, J. Chen, R. Jin, Y. Bai, Y. Zhou, X. Chen, Redox-responsive supramolecular micelles for targeted imaging and drug delivery to tumor, J. Biomed. Nanotechnol. 14 (2018) 1107–1116.
[34] J. Liao, X. Wei, B. Ran, J. Peng, Y. Qu, Z. Qian, Polymer hybrid magnetic nanocapsules encapsulating IR820 and PTX for external magnetic field-guided tumor targeting and multifunctional theranostics, Nanoscale 9 (2017) 2479–2491.
[35] J. Choi, E. Rustique, M. Henry, M. Guidetti, V. Josserand, L. Sancey, J. Boutet, J.L. Coll, Targeting tumors with cyclic RGD-conjugated lipid nanoparticles loaded with an IR780 NIR dye: In vitro and in vivo evaluation, Int. J. Pharm. 532 (2017) 677–685.
[36] J. Liu, T. Lecuyer, J. Seguin, N. Mignet, D. Scherman, B. Viana, C. Richard, Imaging and therapeutic applications of persistent luminescence nanomaterials, Adv. Drug Deliv. Rev. (2018)https://doi.org/10.1016/j.addr.2018.1010.1015.
[37] Q. Miao, K. Pu, Organic semiconducting agents for deep-tissue molecular imaging: Second near-infrared fluorescence, self-luminescence, and photoacoustics, Adv. Mater. 30 (2018), e1801778.
[38] L. Lu, Z.Y. Wu, X. Li, F. Han, State-of-the-art: functional fluorescent probes for bioimaging and pharmacological research, Acta Pharmacol. Sin. (2018)https://doi.org/10.1038/s41401-41018-40190-41408.
[39] J. Qi, C. Chen, D. Ding, B.Z. Tang, Aggregation-induced emission luminogens: Union is strength, gathering illuminates healthcare, Adv. Healthc. Mater. 7 (2018), e1800477.
[40] T. Wang, L. Wang, X. Li, X. Hu, Y. Han, Y. Luo, Z. Wang, Q. Li, A. Aldalbahi, L. Wang, S. Song, C. Fan, Y. Zhao, M. Wang, N. Chen, Size-Dependent Regulation of Intracellular Trafficking of Polystyrene Nanoparticle-Based Drug-Delivery Systems, ACS Appl. Mater. Interfaces 9 (2017) 18619–18625.
[41] M. Pellach, S. Margel, Preparation and characterization of uniform near IR polystyrene nanoparticles, Photochem. Photobiol. 90 (2014) 952–956.
[42] C.P. Hollis, H.L. Weiss, M. Leggas, B.M. Evers, R.A. Gemeinhart, T. Li, Biodistribution and bioimaging studies of hybrid paclitaxel nanocrystals: lessons learned of the EPR effect and image-guided drug delivery, J. Control. Release 172 (2013) 12–21.
[43] Y. Lu, J. Qi, X. Dong, W. Zhao, W. Wu, The in vivo fate of nanocrystals, Drug Discov. Today 22 (2017) 744–750.
[44] Y. Lu, Y. Li, W. Wu, Injected nanocrystals for targeted drug delivery, Acta Pharm. Sin. B 6 (2016) 106–113.
[45] B. Lee, B.G. Park, W. Cho, H.Y. Lee, A. Olasz, C.H. Chen, S.B. Park, D. Lee, BOIMPY: Fluorescent boron complexes with tunable and environment-responsive light-emitting properties, Chemistry 22 (2016) 17321–17328.
[46] P. Sarder, D. Maji, S. Achilefu, Molecular probes for fluorescence lifetime imaging, Bioconjug. Chem. 26 (2015) 963–974.
[47] Z. Yang, J. Cao, Y. He, J.H. Yang, T. Kim, X. Peng, J.S. Kim, Macro-/micro-environment-sensitive chemosensing and biological imaging, Chem. Soc. Rev. 43 (2014) 4563–4601.
[48] A. Suetsugu, M. Shimizu, S. Saji, H. Moriwaki, R.M. Hoffman, Visualizing the tumor microenvironment by color-coded imaging in orthotopic mouse models of cancer, Anticancer Res. 38 (2018) 1847–1857.
[49] M.Z. Abadjian, W.B. Edwards, C.J. Anderson, Imaging the yumor microenvironment, Adv. Exp. Med. Biol. 1036 (2017) 229–257.
[50] N. Gao, W. Yang, H. Nie, Y. Gong, J. Jing, L. Gao, X. Zhang, Turn-on theranostic fluorescent nanoprobe by electrostatic self-assembly of carbon dots with doxorubicin for targeted cancer cell imaging, in vivo hyaluronidase analysis, and targeted drug delivery, Biosens. Bioelectron. 96 (2017) 300–307.
[51] X. Yang, S. Shen, L. Guo, J. Tan, H. Lei, J. Wu, L. Zhao, T. Xiong, Y. Wu, Y. Cheng, Y. Zhang, An enzyme-responsive "Turn-on" fluorescence polymeric superamphiphile as a potential visualizable phosphate prodrug delivery vehicle, Macromol. Biosci. 18 (2018), e1800045.
[52] Y. He, J. Zhou, S. Ma, Y. Nie, D. Yue, Q. Jiang, A.R. Wali, J.Z. Tang, Z. Gu, Multi-responsive "Turn-On" nanocarriers for efficient site-specific gene delivery in vitro and in vivo, Adv. Healthc. Mater. 5 (2016) 2799–2812.
[53] X. Liu, M. Wu, Q. Hu, H. Bai, S. Zhang, Y. Shen, G. Tang, Y. Ping, Redox-activated light-up nanomicelle for precise imaging-guided cancer therapy and real-time pharmacokinetic monitoring, ACS Nano 10 (2016) 11385–11396.
[54] Y. Wang, Y. Zhang, J. Wang, X.J. Liang, Aggregation-induced emission (AIE) fluorophores as imaging tools to trace the biological fate of nano-based drug delivery systems, Adv. Drug Deliv. Rev. (2018)https://doi.org/10.1016/j.addr.2018.1012.1004.
[55] J.B. Birks, Photophysics of aromatic molecules, Wiley- InterScience, London, 1970.
[56] D. Zhai, W. Xu, L. Zhang, Y.T. Chang, The role of "disaggregation" in optical probe development, Chem. Soc. Rev. 43 (2014) 2402–2411.
[57] N. Calander, Theory and simulation of surface plasmon-coupled directional emission from fluorophores at planar structures, Anal. Chem. 76 (2004) 2168–2173.
[58] B. Valeur, M.N. Berberan-Santos, Molecular fluorescence: principles and applications, John Wiley & Sons, Weinheim, 2012.
[59] X. Ma, R. Sun, J. Cheng, J. Liu, F. Gou, H. Xiang, X. Zhou, Fluorescence aggregation-caused quenching versus aggregation-induced emission: A visual teaching technology for undergraduate chemistry students, J. Chem. Educ. 93 (2015) 345–350.
[60] A.C. Grimsdale, K.L. Chan, R.E. Martin, P.G. Jokisz, A.B. Holmes, Synthesis of light-emitting conjugated polymers for applications in electroluminescent devices, Chem. Rev. 109 (2009) 897–1091.
[61] T. Förster, K. Kasper, Ein konzentrationsumschlag der fluoreszenz des pyrens, Z. Phys. Chem. (Munich) 59 (1955) 976–980.

[62] R. Hu, N.L. Leung, B.Z. Tang, AIE macromolecules: syntheses, structures and functionalities, Chem. Soc. Rev. 43 (2014) 4494–4562.
[63] N. Zhao, J.W. Lam, H.H. Sung, H.M. Su, I.D. Williams, K.S. Wong, B.Z. Tang, Effect of the counterion on light emission: a displacement strategy to change the emission behaviour from aggregation-caused quenching to aggregation-induced emission and to construct sensitive fluorescent sensors for Hg^{2+} detection, Chemistry 20 (2014) 133–138.
[64] Y. Hong, J.W. Lam, B.Z. Tang, Aggregation-induced emission: phenomenon, mechanism and applications, Chem. Commun. (2009) 4332–4353.
[65] T.M. Figueira-Duarte, K. Mullen, Pyrene-based materials for organic electronics, Chem. Rev. 111 (2011) 7260–7314.
[66] Z. Guo, W. Zhu, H. Tian, Dicyanomethylene-4H-pyran chromophores for OLED emitters, logic gates and optical chemosensors, Chem. Commun. 48 (2012) 6073–6084.
[67] S. Setayesh, A.C. Grimsdale, T. Weil, V. Enkelmann, K. Mullen, F. Meghdadi, E.J. List, G. Leising, Polyfluorenes with polyphenylene dendron side chains: toward non-aggregating, light-emitting polymers, J. Am. Chem. Soc. 123 (2001) 946–953.
[68] M. Huang, R. Yu, K. Xu, S. Ye, S. Kuang, X. Zhu, Y. Wan, An arch-bridge-type fluorophore for bridging the gap between aggregation-caused quenching (ACQ) and aggregation-induced emission (AIE), Chem. Sci. 7 (2016) 4485–4491.
[69] F. Meng, J. Wang, Q. Ping, Y. Yeo, Quantitative assessment of nanoparticle biodistribution by fluorescence imaging, revisited, ACS Nano 12 (2018) 6458–6468.
[70] J. Kunzler, L. Samha, R. Zhang, H. Samha, Investigation of the effect of concentration on molecular aggregation of cyanine dyes in aqueous solution, Am. J. Undegrad. Res. 9 (2011) 1–4.
[71] Y. Hong, J.W. Lam, B.Z. Tang, Aggregation-induced emission, Chem. Soc. Rev. 40 (2011) 5361–5388.
[72] X. Hu, J. Zhang, Z. Yu, Y. Xie, H. He, J. Qi, X. Dong, Y. Lu, W. Zhao, W. Wu, Environment-responsive aza-BODIPY dyes quenching in water as potential probes to visualize the in vivo fate of lipid-based nanocarriers, Nanomedicine 11 (2015) 1939–1948.
[73] C. Ren, H. Wang, D. Mao, X. Zhang, Q. Fengzhao, Y. Shi, D. Ding, D. Kong, L. Wang, Z. Yang, When molecular probes meet self-assembly: an enhanced quenching effect, Angew. Chem. Int. Ed. 54 (2015) 4823–4827.
[74] B. Fu, J. Huang, D. Bai, Y. Xie, Y. Wang, S. Wang, X. Zhou, Label-free detection of pH based on the i-motif using an aggregation-caused quenching strategy, Chem. Commun. 51 (2015) 16960–16963.
[75] W.Z. Yuan, P. Lu, S. Chen, J.W. Lam, Z. Wang, Y. Liu, H.S. Kwok, Y. Ma, B.Z. Tang, Changing the behavior of chromophores from aggregation-caused quenching to aggregation-induced emission: Development of highly efficient light emitters in the solid state, Adv. Mater. 22 (2010) 2159–2163.
[76] B.S. Li, H. Li, B.Z. Tang, Molecular design, Circularly polarized and helical self-assembly of chiral aggregation induced emission molecules, Chem. Asian J. (2018)https://doi.org/10.1002/asia.201801469.
[77] Y. Dong, B. Liu, Y. Yuan, AIEgen based drug delivery systems for cancer therapy, J. Control. Release 290 (2018) 129–137.
[78] M. Gao, B.Z. Tang, Aggregation-induced emission probes for cancer theranostics, Drug Discov. Today 22 (2017) 1288–1294.
[79] S.W. Thomas, G.D. Joly, T.M. Swager, Chemical sensors based on amplifying fluorescent conjugated polymers, Chem. Rev. 107 (2007) 1339–1386.
[80] G. Behera, P. Behera, B.K. Mishra, Cyanine dyes: self aggregation and behaviour in surfactants a review, J. Surf. Sci. Technol. 23 (2007) 1.
[81] D. Zhai, W. Xu, L. Zhang, Y.-T. Chang, The role of "disaggregation" in optical probe development, Chem. Soc. Rev. 43 (2014) 2402–2411.
[82] U. Rösch, S. Yao, R. Wortmann, F. Würthner, Fluorescent H-aggregates of merocyanine dyes, Angew. Chem. 118 (2006) 7184–7188.
[83] M. Reers, T.W. Smith, L.B. Chen, J-aggregate formation of a carbocyanine as a quantitative fluorescent indicator of membrane potential, Biochemistry 30 (1991) 4480–4486.
[84] W.J. Harrison, D.L. Mateer, G.J. Tiddy, Liquid-crystalline J-aggregates formed by aqueous ionic cyanine dyes, J. Phys. Chem. 100 (1996) 2310–2321.
[85] P. Wheatley, The crystallography of some cyanine dyes, J. Chem. Soc. (1959) 3245–3250.
[86] J.L. Bricks, Y.L. Slominskii, I.D. Panas, A.P. Demchenko, Fluorescent J-aggregates of cyanine dyes: basic research and applications review, Methods Appl. Fluorensc. 6 (2017), 012001.
[87] C. Tan, M.R. Pinto, K.S. Schanze, Photophysics, aggregation and amplified quenching of a water-soluble poly (phenylene ethynylene), Chem. Commun. (2002) 446–447.
[88] Z.-Q. Liang, Y.-X. Li, J.-X. Yang, Y. Ren, X.-T. Tao, Suppression of aggregation-induced fluorescence quenching in pyrene derivatives: photophysical properties and crystal structures, Tetrahedron Lett. 52 (2011) 1329–1333.
[89] M.M. Amiji, Pyrene fluorescence study of chitosan self-association in aqueous solution, Carbohydr. Polym. 26 (1995) 211–213.
[90] K. Kalyanasundaram, J. Thomas, Environmental effects on vibronic band intensities in pyrene monomer fluorescence and their application in studies of micellar systems, J. Am. Chem. Soc. 99 (1977) 2039–2044.
[91] J. Weinstein, S. Yoshikami, P. Henkart, R. Blumenthal, W. Hagins, Liposome-cell interaction: transfer and intracellular release of a trapped fluorescent marker, Science 195 (1977) 489–492.
[92] S. Hamann, J.F. Kiilgaard, T. Litman, F.J. Alvarez-Leefmans, B.R. Winther, T. Zeuthen, Measurement of cell volume changes by fluorescence self-quenching, J. Fluoresc. 12 (2002) 139–145.
[93] S. Chakraborty, P. Debnath, D. Dey, D. Bhattacharjee, S.A. Hussain, Formation of fluorescent H-aggregates of a cyanine dye in ultrathin film and its effect on energy transfer, J. Photochem. Photobiol. A: Chem. 293 (2014) 57–64.
[94] Y. Li, D. Xu, A. Sun, S.L. Ho, C.Y. Poon, H.N. Chan, O. Ng, K. Yung, H. Yan, H.W. Li, Fluoro-substituted cyanine for reliable in vivo labelling of amyloid-β oligomers and neuroprotection against amyloid-β induced toxicity, Chem. Sci. 8 (2017) 8279.
[95] H. He, J. Zhang, Y. Xie, Y. Lu, J. Qi, E. Ahmad, X. Dong, W. Zhao, W. Wu, Bioimaging of intravenous polymeric micelles based on discrimination of integral particles using an environment-responsive probe, Mol. Pharm. 13 (2016) 4013–4019.
[96] Y. Xie, X. Hu, H. He, F. Xia, Y. Ma, J. Qi, X. Dong, W. Zhao, Y. Lu, W. Wu, Tracking translocation of glucan microparticles targeting M cells: implications for oral drug delivery, J. Mater. Chem. B 4 (2016) 2864–2873.
[97] F. Xia, W. Fan, S. Jiang, Y. Ma, Y. Lu, J. Qi, E. Ahmad, X. Dong, W. Zhao, W. Wu, Size-dependent translocation of nanoemulsions via oral delivery, ACS Appl. Mater. Interfaces 9 (2017) 21660–21672.
[98] U. Resch-Genger, M. Grabolle, S. Cavaliere-Jaricot, R. Nitschke, T. Nann, Quantum dots versus organic dyes as fluorescent labels, Nat. Methods 5 (2008) 763.
[99] V.V. Breus, C.D. Heyes, G.U. Nienhaus, Quenching of CdSe—ZnS core—shell quantum dot luminescence by water-soluble thiolated ligands, J. Phys. Chem. C 111 (2007) 18589–18594.
[100] S. Chen, J.-W. Liu, M.-L. Chen, X.-W. Chen, J.-H. Wang, Unusual emission transformation of graphene quantum dots induced by self-assembled aggregation, Chem. Commun. 48 (2012) 7637–7639.
[101] J. Liu, X. Yang, K. Wang, R. Yang, H. Ji, L. Yang, C. Wu, A switchable fluorescent quantum dot probe based on aggregation/disaggregation mechanism, Chem. Commun. 47 (2011) 935–937.
[102] M. Noh, T. Kim, H. Lee, C.-K. Kim, S.-W. Joo, K. Lee, Fluorescence quenching caused by aggregation of water-soluble CdSe quantum dots, Colloids Surf. A Physicochem. Eng. Asp. 359 (2010) 39–44.
[103] L. Yan, Y. Zhang, B. Xu, W. Tian, Fluorescent nanoparticles based on AIE fluorogens for bioimaging, Nanoscale 8 (2016) 2471–2487.
[104] Z. Guo, S. Park, J. Yoon, I. Shin, Recent progress in the development of near-infrared fluorescent probes for bioimaging applications, Chem. Soc. Rev. 43 (2014) 16–29.
[105] R. Bouchaala, L. Mercier, B. Andreiuk, Y. Mély, T. Vandamme, N. Anton, J.G. Goetz, A.S. Klymchenko, Integrity of lipid nanocarriers in bloodstream and tumor quantified by near-infrared ratiometric FRET imaging in living mice, J. Control. Release 236 (2016) 57–67.
[106] C. Shen, Y. Yang, B. Shen, Y. Xie, J. Qi, X. Dong, W. Zhao, W. Zhu, W. Wu, H. Yuan, Self-discriminating fluorescent hybrid nanocrystals: efficient and accurate tracking of translocation via oral delivery, Nanoscale 10 (2018) 436–450.
[107] H. Mu, C.E. Hoy, The digestion of dietary triacylglycerols, Prog. Lipid Res. 43 (2004) 105–133.
[108] C.J. Porter, N.L. Trevaskis, W.N. Charman, Lipids and lipid-based formulations: optimizing the oral delivery of lipophilic drugs, Nat. Rev. Drug Discov. 6 (2007) 231–248.
[109] M.A. Hahn, A.K. Singh, P. Sharma, S.C. Brown, B.M. Moudgil, Nanoparticles as contrast agents for in-vivo bioimaging: current status and future perspectives, Anal. Bioanal. Chem. 399 (2011) 3–27.
[110] A. Reisch, A.S. Klymchenko, Fluorescent polymer nanoparticles based on dyes: seeking brighter tools for bioimaging, Small 12 (2016) 1968–1992.
[111] R. Wang, L. Zhou, W. Wang, X. Li, F. Zhang, In vivo gastrointestinal drug-release monitoring through second near-infrared window fluorescent bioimaging with orally delivered microcarriers, Nat. Commun. 8 (2017), 14702.
[112] X. Hu, W. Fan, Z. Yu, Y. Lu, J. Qi, J. Zhang, X. Dong, W. Zhao, W. Wu, Evidence does not support absorption of intact solid lipid nanoparticles via oral delivery, Nanoscale 8 (2016) 7024–7035.
[113] C. Eggeling, J. Widengren, R. Rigler, C. Seidel, Photobleaching of fluorescent dyes under conditions used for single-molecule detection: Evidence of two-step photolysis, Anal. Chem. 70 (1998) 2651–2659.
[114] S. Cheung, D.F. O'Shea, Directed self-assembly of fluorescence responsive nanoparticles and their use for real-time surface and cellular imaging, Nat. Commun. 8 (2017) 1885.
[115] H. Nie, K. Hu, Y. Cai, Q. Peng, Z. Zhao, R. Hu, J. Chen, S.-J. Su, A. Qin, B.Z. Tang, Tetraphenylfuran: aggregation-induced emission or aggregation-caused quenching? Mat. Chem. Front. 1 (2017) 1125–1129.
[116] L. Piñeiro, M. Novo, W. Al-Soufi, Fluorescence emission of pyrene in surfactant solutions, Adv. Colloid Interf. Sci. 215 (2015) 1–12.
[117] H. He, S. Jiang, Y. Xie, Y. Lu, J. Qi, X. Dong, W. Zhao, Z. Yin, W. Wu, Reassessment of long circulation via monitoring of integral polymeric nanoparticles justifies a more accurate understanding, Nanoscale Horiz. 3 (2018) 397–407.
[118] N. Kamaly, B. Yameen, J. Wu, O.C. Farokhzad, Degradable controlled-release polymers and polymeric nanoparticles: mechanisms of controlling drug release, Chem. Rev. 116 (2016) 2602–2663.
[119] Y. Ma, H. He, F. Xia, Y. Li, Y. Lu, D. Chen, J. Qi, Y. Lu, W. Zhang, W. Wu, In vivo fate of lipid-silybin conjugate nanoparticles: Implications on enhanced oral bioavailability, Nanomedicine 13 (2017) 2643–2654.
[120] Y. Ma, H. He, W. Fan, Y. Li, W. Zhang, W. Zhao, J. Qi, Y. Lu, X. Dong, W. Wu, In vivo fate of biomimetic mixed micelles as nanocarriers for bioavailability enhancement of lipid–drug conjugates, ACS Biomat. Sci. Eng. 3 (2017) 2399–2409.
[121] E. Ahmad, Y. Feng, J. Qi, W. Fan, Y. Ma, H. He, F. Xia, X. Dong, W. Zhao, Y. Lu, Evidence of nose-to-brain delivery of nanoemulsions: cargoes but not vehicles, Nanoscale 9 (2017) 1174–1183.
[122] Z. Tian, Q. Yu, Y. Xie, F. Li, Y. Lu, X. Dong, W. Zhao, J. Qi, W. Wu, Controlling release of integral lipid nanoparticles based on osmotic pump technology, Pharm. Res. 33 (2016) 1988–1997.

[123] M. Cui, W. Wu, L. Hovgaard, Y. Lu, D. Chen, J. Qi, Liposomes containing cholesterol analogues of botanical origin as drug delivery systems to enhance the oral absorption of insulin, Int. J. Pharm. 489 (2015) 277–284.
[124] Y. Xie, S. Jiang, F. Xia, X. Hu, H. He, Z. Yin, J. Qi, Y. Lu, W. Wu, Glucan microparticles thickened with thermosensitive gels as potential carriers for oral delivery of insulin, J. Mater. Chem. B 4 (2016) 4040–4048.
[125] L.A. Lane, X. Qian, A.M. Smith, S. Nie, Physical chemistry of nanomedicine: understanding the complex behaviors of nanoparticles in vivo, Annu. Rev. Phys. Chem. 66 (2015) 521–547.
[126] J. Qi, Y. Lu, W. Wu, Absorption, disposition and pharmacokinetics of solid lipid nanoparticles, Curr. Drug Metab. 13 (2012) 418–428.
[127] A. Beloqui, M.A. Solinis, A.R. Gascon, A. del Pozo-Rodriguez, A. des Rieux, V. Preat, Mechanism of transport of saquinavir-loaded nanostructured lipid carriers across the intestinal barrier, J. Control. Release 166 (2013) 115–123.
[128] C. Chen, T. Fan, Y. Jin, Z. Zhou, Y. Yang, X. Zhu, Z.R. Zhang, Q. Zhang, Y. Huang, Orally delivered salmon calcitonin-loaded solid lipid nanoparticles prepared by micelle-double emulsion method via the combined use of different solid lipids, Nanomedicine 8 (2013) 1085–1100.
[129] Z. Zhang, F. Gao, H. Bu, J. Xiao, Y. Li, Solid lipid nanoparticles loading candesartan cilexetil enhance oral bioavailability: in vitro characteristics and absorption mechanism in rats, Nanomedicine 8 (2012) 740–747.
[130] G.-H. Chai, Y. Xu, S.-Q. Chen, B. Cheng, F.-Q. Hu, J. You, Y.-Z. Du, H. Yuan, Transport mechanisms of solid lipid nanoparticles across Caco-2 cell monolayers and their related cytotoxicology, ACS Appl. Mater. Interfaces 8 (2016) 5929–5940.
[131] P. Li, H.M. Nielsen, A. Müllertz, Impact of lipid-based drug delivery systems on the transport and uptake of insulin across Caco-2 cell monolayers, J. Pharm. Sci. 105 (2016) 2743–2751.
[132] Y. Singh, J.G. Meher, K. Raval, F.A. Khan, M. Chaurasia, N.K. Jain, M.K. Chourasia, Nanoemulsion: Concepts, development and applications in drug delivery, J. Control. Release 252 (2017) 28–49.
[133] L. Salvia-Trujillo, O. Martín-Belloso, D.J. McClements, Excipient nanoemulsions for improving oral bioavailability of bioactives, Nanomaterials 6 (2016) 17.
[134] Y. Gao, W. Zhang, T. Sun, Local transdermal delivery of 10, 11-methylenedioxycamptothecin by nanoemulsion for breast cancer prevention, J. Control. Release 259 (2017) e180–e181.
[135] A. Banerjee, J. Qi, R. Gogoi, J. Wong, S. Mitragotri, Role of nanoparticle size, shape and surface chemistry in oral drug delivery, J. Control. Release 238 (2016) 176–185.
[136] C. He, L. Yin, C. Tang, C. Yin, Size-dependent absorption mechanism of polymeric nanoparticles for oral delivery of protein drugs, Biomaterials 33 (2012) 8569–8578.
[137] K. Baert, B.G. De Geest, R. De Rycke, A.B. da Fonseca Antunes, H. De Greve, E. Cox, B. Devriendt, β-Glucan microparticles targeted to epithelial APN as oral antigen delivery system, J. Control. Release 220 (2015) 149–159.
[138] E. Soares, S. Jesus, O. Borges, Oral hepatitis B vaccine: chitosan or glucan based delivery systems for efficient HBsAg immunization following subcutaneous priming, Int. J. Pharm. 535 (2018) 261–271.
[139] S. Iqbal, X. Du, J. Wang, H. Li, Y. Yuan, J. Wang, Surface charge tunable nanoparticles for TNF-α siRNA oral delivery for treating ulcerative colitis, Nano Res. 11 (2018) 2872–2884.
[140] M. De Jesus, G.R. Ostroff, S.M. Levitz, T.R. Bartling, N.J. Mantis, A population of Langerin-positive dendritic cells in murine Peyer's patches involved in sampling β-glucan microparticles, PLoS One 9 (2014), e91002.
[141] J. Qi, J. Zhuang, Y. Lv, Y. Lu, W. Wu, Exploiting or overcoming the dome trap for enhanced oral immunization and drug delivery, J. Control. Release 275 (2018) 92–106.
[142] E.M. Pridgen, F. Alexis, O.C. Farokhzad, Polymeric nanoparticle drug delivery technologies for oral delivery applications, Expert Opin. Drug Deliv. 12 (2015) 1459–1473.
[143] P. Fonte, F. Araújo, C. Silva, C. Pereira, S. Reis, H.A. Santos, B. Sarmento, Polymer-based nanoparticles for oral insulin delivery: Revisited approaches, Biotechnol. Adv. 33 (2015) 1342–1354.
[144] H. He, Y. Xie, Y. Lv, J. Qi, X. Dong, W. Zhao, W. Wu, Y. Lu, Bioimaging of intact polycaprolactone nanoparticles using aggregation-caused quenching probes: size-dependent translocation via oral delivery, Adv. Healthc. Mater. 7 (2018), e1800711.
[145] V.B. Junyaprasert, B. Morakul, Nanocrystals for enhancement of oral bioavailability of poorly water-soluble drugs, Asian J. Pharm. Sci. 10 (2015) 13–23.
[146] V.K. Pawar, Y. Singh, J.G. Meher, S. Gupta, M.K. Chourasia, Engineered nanocrystal technology: in-vivo fate, targeting and applications in drug delivery, J. Control. Release 183 (2014) 51–66.
[147] Y. Gao, C. Wang, M. Sun, X. Wang, A. Yu, A. Li, G. Zhai, In vivo evaluation of curcumin loaded nanosuspensions by oral administration, J. Biomed. Nanotechnol. 8 (2012) 659–668.
[148] Y. Xie, B. Shi, F. Xia, J. Qi, X. Dong, W. Zhao, T. Li, W. Wu, Y. Lu, Epithelia transmembrane transport of orally administered ultrafine drug particles evidenced by environment sensitive fluorophores in cellular and animal studies, J. Control. Release 270 (2018) 65–75.
[149] S. Wilhelm, A.J. Tavares, Q. Dai, S. Ohta, J. Audet, H.F. Dvorak, W.C. Chan, Analysis of nanoparticle delivery to tumours, Nat. Rev. Mat. 1 (2016), 16014.
[150] Z. He, X. Wan, A. Schulz, H. Bludau, M.A. Dobrovolskaia, S.T. Stern, S.A. Montgomery, H. Yuan, Z. Li, D. Alakhova, A high capacity polymeric micelle of paclitaxel: Implication of high dose drug therapy to safety and in vivo anti-cancer activity, Biomaterials 101 (2016) 296–309.
[151] H.K. Ahn, M. Jung, S.J. Sym, D.B. Shin, S.M. Kang, S.Y. Kyung, J.-W. Park, S.H. Jeong, E.K. Cho, A phase II trial of Cremorphor EL-free paclitaxel (Genexol-PM) and gemcitabine in patients with advanced non-small cell lung cancer, Cancer Chemother. Pharmacol. 74 (2014) 277–282.
[152] Y. Zhang, Q. Li, W.J. Welsh, P.V. Moghe, K.E. Uhrich, Micellar and structural stability of nanoscale amphiphilic polymers: implications for anti-atherosclerotic bioactivity, Biomaterials 84 (2016) 230–240.
[153] S.W. Morton, X. Zhao, M.A. Quadir, P.T. Hammond, FRET-enabled biological characterization of polymeric micelles, Biomaterials 35 (2014) 3489–3496.
[154] X. Sun, G. Wang, H. Zhang, S. Hu, X. Liu, J. Tang, Y. Shen, The blood clearance kinetics and pathway of polymeric micelles in cancer drug delivery, ACS Nano 12 (2018) 6179–6192.
[155] K. Sakai-Kato, N. Nishiyama, M. Kozaki, T. Nakanishi, Y. Matsuda, M. Hirano, H. Hanada, S. Hisada, H. Onodera, H. Harashima, General considerations regarding the in vitro and in vivo properties of block copolymer micelle products and their evaluation, J. Control. Release 210 (2015) 76–83.
[156] X.-Y. Ke, V.W.L. Ng, S.-J. Gao, Y.W. Tong, J.L. Hedrick, Y.Y. Yang, Co-delivery of thioridazine and doxorubicin using polymeric micelles for targeting both cancer cells and cancer stem cells, Biomaterials 35 (2014) 1096–1108.
[157] K. Shao, Y. Zhang, N. Ding, S. Huang, J. Wu, J. Li, C. Yang, Q. Leng, L. Ye, J. Lou, Functionalized nanoscale micelles with brain targeting ability and intercellular microenvironment biosensitivity for anti-intracranial infection applications, Adv. Healthc. Mater. 4 (2015) 291–300.
[158] W. Gao, D. Lee, Z. Meng, T. Li, Exploring intracellular fate of drug nanocrystals with crystal-integrated and environment-sensitive fluorophores, J. Control. Release 267 (2017) 214–222.
[159] T. Wang, J. Qi, N. Ding, X. Dong, W. Zhao, Y. Lu, C. Wang, W. Wu, Tracking translocation of self-discriminating curcumin hybrid nanocrystals following intravenous delivery, Int. J. Pharm. 546 (2018) 10–19.
[160] S. Wiedersberg, R.H. Guy, Transdermal drug delivery: 30+ years of war and still fighting! J. Control. Release 190 (2014) 150–156.
[161] B. Das Kurmi, P. Tekchandani, R. Paliwal, S. Rai Paliwal, Transdermal drug delivery: Opportunities and challenges for controlled delivery of therapeutic agents using nanocarriers, Curr. Drug Metab. 18 (2017) 481–495.
[162] R. Su, W. Fan, Q. Yu, X. Dong, J. Qi, Q. Zhu, W. Zhao, W. Wu, Z. Chen, Y. Li, Size-dependent penetration of nanoemulsions into epidermis and hair follicles: implications for transdermal delivery and immunization, Oncotarget 8 (2017), 38214.
[163] Y. Feng, H. He, F. Li, Y. Lu, J. Qi, W. Wu, An update on the role of nanovehicles in nose-to-brain drug delivery, Drug Discov. Today 23 (2018) 1079–1088.
[164] E. Muntimadugu, R. Dhommati, A. Jain, V.G.S. Challa, M. Shaheen, W. Khan, Intranasal delivery of nanoparticle encapsulated tarenflurbil: A potential brain targeting strategy for Alzheimer's disease, Eur. J. Pharm. Sci. 92 (2016) 224–234.
[165] J.J. Lochhead, D.J. Wolak, M.E. Pizzo, R.G. Thorne, Rapid transport within cerebral perivascular spaces underlies widespread tracer distribution in the brain after intranasal administration, J. Cereb. Blood Flow Metab. 35 (2015) 371–381.
[166] M. Hussain, R.M. Shtein, A. Sugar, H.K. Soong, M.A. Woodward, K. DeLoss, S.I. Mian, Long-term use of autologous serum 50% eye drops for the treatment of dry eye disease, Cornea 33 (2014) 1245–1251.
[167] I.P. Kaur, S. Kakkar, Nanotherapy for posterior eye diseases, J. Control. Release 193 (2014) 100–112.
[168] N.C. Steinle, D.S. Dhoot, C.Q. Ruiz, A.A. Castellarin, D.J. Pieramici, R.F. See, S.C. Couvillion, A.N. Ma'an, R.L. Avery, Treatment of vitreomacular traction with intravitreal perfluoropropane (C3F8) injection, Retina 37 (2017) 643–650.
[169] P. Chetoni, S. Burgalassi, D. Monti, S. Tampucci, V. Tullio, A.M. Cuffini, E. Muntoni, R. Spagnolo, G.P. Zara, R. Cavalli, Solid lipid nanoparticles as promising tool for intraocular tobramycin delivery: Pharmacokinetic studies on rabbits, Eur. J. Pharm. Biopharm. 109 (2016) 214–223.
[170] I. Bravo-Osuna, V. Andrés-Guerrero, A. Arranz-Romera, S. Esteban-Pérez, I.T. Molina-Martínez, R. Herrero-Vanrell, Microspheres as intraocular therapeutic tools in chronic diseases of the optic nerve and retina, Adv. Drug Deliv. Rev. 126 (2018) 127–144.
[171] B. Wan, Y. Dai, D. Liu, J. Qi, X. Dong, W. Zhao, W. Wu, Y. Lu, Intraocular fate of polycaprolactone nanoparticles administered via intravitreal and various periocular routes: Bioimaging of integral nanoparticles using environment-sensitive fluorophores, J. Biomed. Nanotechnol. 13 (2017) 960–972.
[172] Z. Huang, Y. Huang, C. Ma, X. Ma, X. Zhang, L. Lin, Z. Zhao, X. Pan, C. Wu, Endotracheal aerosolization device for laboratory investigation of pulmonary delivery of nanoparticle suspensions: In vitro and in vivo validation, Mol. Pharm. 15 (2018) 5521–5533.
[173] Y. Lv, H. He, J. Qi, Y. Lu, W. Zhao, X. Dong, W. Wu, Visual validation of the measurement of entrapment efficiency of drug nanocarriers, Int. J. Pharm. 547 (2018) 395–403.